

12-2014

Development, Analysis, and Comparison of Electromechanical Properties and Electrode Morphology of Ionic Polymer Metal Composites

Balaji Sivasubramanian

Follow this and additional works at: <https://commons.erau.edu/edt>



Part of the [Aerospace Engineering Commons](#)

Scholarly Commons Citation

Sivasubramanian, Balaji, "Development, Analysis, and Comparison of Electromechanical Properties and Electrode Morphology of Ionic Polymer Metal Composites" (2014). *Dissertations and Theses*. 284.
<https://commons.erau.edu/edt/284>

This Thesis - Open Access is brought to you for free and open access by Scholarly Commons. It has been accepted for inclusion in Dissertations and Theses by an authorized administrator of Scholarly Commons. For more information, please contact commons@erau.edu.

DEVELOPMENT, ANALYSIS, AND COMPARISON OF ELECTROMECHANICAL
PROPERTIES AND ELECTRODE MORPHOLOGY OF IONIC POLYMER METAL
COMPOSITES

By

Balaji Sivasubramanian

A Thesis Submitted to the College of Engineering Department of Aerospace Engineering
in Partial Fulfillment of the Requirements for the Degree of
Master of Science in Aerospace Engineering

Embry-Riddle Aeronautical University
Daytona Beach, Florida
December 2014

DEVELOPMENT, ANALYSIS, AND COMPARISON OF ELECTROMECHANICAL
PROPERTIES AND ELECTRODE MORPHOLOGY OF IONIC POLYMER METAL
COMPOSITES

By

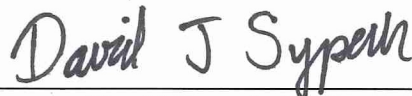
Balaji Sivasubramanian

This thesis was prepared under the direction of the candidate's Thesis Committee Chair,
Dr. Daewon Kim, Assistant Professor, Daytona Beach Campus and Thesis Committee
Members Dr. David Sypeck, Professor, Daytona Beach Campus and
Dr. Emily Faulconer, Assistant Professor, Daytona Beach Campus, and
has been approved by the Thesis Committee. It was submitted to the
Department of Aerospace Engineering in partial
fulfillment of the requirements for the degree of
Master of Science in Aerospace Engineering

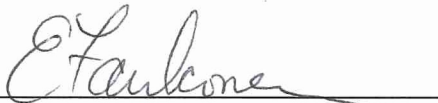
Thesis Review Committee:



DaeWon Kim, Ph.D.
Committee Chair



David Sypeck, Ph.D.
Committee Member



Emily Faulconer, Ph.D.
Committee Member



Yi Zhao, Ph.D.
Graduate Program Chair



Robert Oxley, Ph.D.
Associate Vice President of Academics

12-8-14

Date

Dedication

To Her.

The cause behind the effect, the reason behind the cause and the energy
behind the reason

Acknowledgements

I would like to take this opportunity to thank everyone who has helped me through my research work and has contributed to finishing this thesis.

I would first like to thank my thesis advisor Dr. Daewon Kim for his kind help and his continuous support throughout my master's degree. If not for him, I would not have gained any knowledge at all. His relentless inspiration and help has kept me going and his push is what has driven me to achieve any little success I have till date. I would like to thank my thesis committee members Dr. David Sypeck, the genius behind the solution to all my engineering problems and Dr. Emily Faulconer without whose help I would not have been able to pursue anything at all with regards to chemistry. My sincere thanks reach out to the Environmental Health & Safety director Justin Grillot who has kept me safe till now throughout the project.

I would also like to thank Mike Potash and Bill Russo whose help in the electronics and mechanical division has been extremely valuable. They have been relentlessly solving my problems for not just this project but every single one I have done in ERAU so far. I would like to thank Dr. Virginie Rollin whose help with Scanning Electron Microscopy and Energy Dispersive X-ray Spectroscopy and the training involved in it has helped me complete this thesis. The use of the Scanning Electron Microscope was made possible through NSF grant 1337742.

I would like to thank my parents Mr. T.S.R. Sivasubramanian and Mrs. Poorna Sivasubramanian for their support and motivation. Without their belief in me I would be nothing. I would also like to thank my sister and brother in law Varna Dheeraj and Dheeraj Kumar Rajamohan for their help and guidance. I would like to thank my friends Boutros Azizi (Peter) for his encouragement and all his help. His support has been the biggest factor that made me get up and walk whenever I was feeling down. Last but not the least; I would like to thank Janani Sridhar – who has always been the biggest motivation for me directly and indirectly.

Abstract

Researcher: Balaji Sivasubramanian

Title: Development, Analysis, and Comparison of Electromechanical Properties and Electrode Morphology of Ionic Polymer Metal Composites

Institution: Embry-Riddle Aeronautical University

Degree: Master of Science in Aerospace Engineering

Year: 2014

With smart materials and adaptive structures being nudged into mainstream technology progressively, the smart composites are donning a predominant role as indispensable structures. Among these, the Ionic Polymer Metal Composites (IPMC), with their large bending deformation and relaxation characteristics at very low voltages are attractive as transducers in many areas of application. The actuation and sensing properties of IPMC have been sought after for various engineering functions. The paper focuses on manufacturing various types of IPMC. Combining the ionic polymer with platinum electrodes, gold sputter coated electrodes and multi-walled carbon nanotube Bucky paper electrodes to create enhanced IPMCs, comparative analysis of different manufacturing methodologies discussing the electrode morphology using scanning electron microscopy and energy dispersive X-ray spectroscopy techniques is studied. A comparison of the uniformity of the electrode plating obtained from the different processes is studied while the research also concentrates on making use of different ionic solutions to change the

anions within the polymer membrane for comparison such as to determine the most suited ion content within the solid electrolyte for effective IPMC actuation. A COMSOL multiphysics model is attempted in this thesis, which effectively describes a multiphysics modeling approach for the IPMC. This new functionally graded material is tested for its bending deformation, blocking force and the current consumption to prove the electro-mechanical efficiency of the platinum, gold and Bucky paper IPMC. By studying the electromechanical properties of this smart composite actuator based on its actuation under different electric excitations, we can draw conclusions subsequently from the results of the comparison.

Table of Contents

Dedication	iii
Acknowledgements	iv
Abstract	v
CHAPTER 1 Introduction	1
1.1 Smart Materials	1
1.2 Types of Smart Materials	2
1.2.1 Piezoelectric Materials	4
1.2.2 Electro Rheological and Magneto Rheological Materials	5
1.2.3 Shape Memory Alloys	7
1.2.4 Chromic Materials	8
1.2.4 Polymer Based Smart Materials	9
CHAPTER 2 Ionic Polymer Metal Composites	13
2.1 Polymer Membrane	14
2.2 Electrodes and Manufacturing	18
2.2.1 Different Types of Electrodes and Plating	18
2.3 Electroless Plating or Chemical Plating	19
2.3.1 Mild Sandblasting and Ultrasonic Treatment	19
2.3.2 The Electroless Plating Method	22

2.3.3	Ion Adsorption -----	23
2.3.4	Primary Plating-----	23
2.3.5	Secondary Plating-----	25
2.4	Direct Assembly Process -----	26
2.4.1	Vacuum treatment -----	27
2.4.2	Ion replacement and Direct Assembly -----	28
2.5	Sputter Coating -----	29
2.5.1	Sample Preparation -----	31
2.5.2	Table Height -----	31
2.5.3	Sputter Settings-----	31
2.5.4	Cylinder and Regulator Settings -----	32
2.5.5	Timer and Sputter Coating -----	32
2.5.6	Ion Exchange -----	33
CHAPTER 3 Finite Element Method – COMSOL Modeling -----		34
3.1	The Modules and Interfaces -----	35
3.1.1	The AC/DC Module -----	35
3.1.2	The Electric Current Interface -----	35
3.1.3	The Electrostatics Interface -----	36
3.1.4	The Batteries and Fuel Cells Module -----	36

3.1.5	The Transport of Diluted Species Interface -----	37
3.2	Modeling-----	37
3.2.1	Geometry-----	38
3.2.2	Materials -----	41
3.3	Mesh-----	45
3.4	Multiphysics-----	48
3.4.1	Free End-----	59
3.4.2	Fixed constraint -----	59
3.5	Results -----	60
CHAPTER 4 Experimental Results -----		64
4.1	Displacement Results -----	68
4.2	Blocking Force and Current Consumption Results-----	76
4.3	Electrode morphology and Failure study-----	79
4.3.1	Gold Electrode Morphology -----	79
4.3.2	Bucky Paper Electrode Morphology -----	85
4.3.3	Platinum Electrode Morphology-----	87
4.3.3	Gold Electrode Failure -----	90
4.3.4	Bucky Paper Electrode Failure and Comparison with Platinum -----	92
CHAPTER 5 Conclusion and Future work-----		97

CHAPTER 1 Introduction

1.1 Smart Materials

The bridge between living and nonliving is the ability to respond, either to a stimulus, such as muscles flinching in pain, or to a particular environment, as how plants grow towards sunlight. Though this is not the single most characteristic difference, it certainly is the most interesting aspect. Generally known as sensory transduction, this form of interaction converts one form of stimulus into another.

Smart materials are those that bridge the gap between living and nonliving on an engineering point of view. Materials that respond to a particular stimulus or a combination of stimuli are known as smart materials. They do not have macroscopic moving parts and do not have conventional moving mechanisms. They rather respond to their environment or a particular stimulus based on their material configuration. They can either be transducers that convert one form of energy into another or produce a large bending deformation.

They can respond to an electric field (widely known as electro active or electrostrictive materials) or can respond to a magnetic field in which they would be considered magnetostrictive or furthermore they can respond to pressure, heat, light or even the pH of their environment.

1.2 Types of Smart Materials

According to literature, smart materials have been around for long though the term has been in use since the 1980s and have been called smart, intelligent or adaptive materials according to various sources [1]. The various types of smart materials are based on the stimulus that they respond to and the fashion in which their response is displayed.

There can be hundreds of different smart materials based on their material properties and their application. The Heckmann diagram shown in Figure 1.1 describes the relation between electric field, mechanical stress and temperature for basic property correlation of major types of smart material transduction. Though it covers major properties, each smart material has its own intricacies and usually the properties that influence them and the properties that the smart materials display are combined and cannot be taken individually.

This means that a certain smart material may display more than a single characteristic transduction such as direct as well as converse piezoelectric effect or ferroelectric and shape memory effects. These cannot be explained with just the Heckmann diagram. Hence a few examples of extensively used smart materials have been given for general understanding.

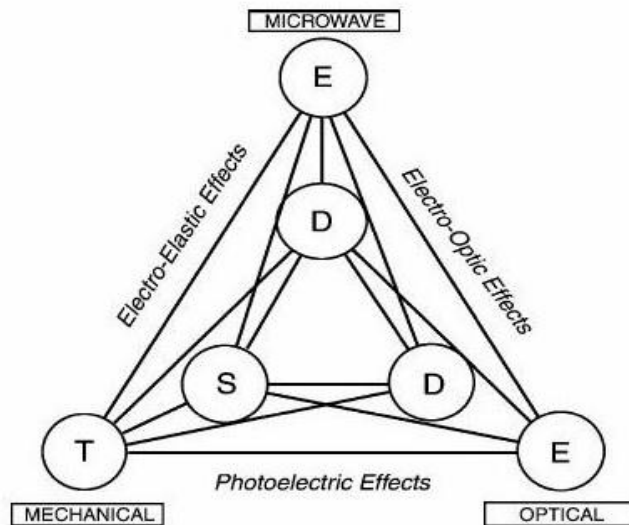
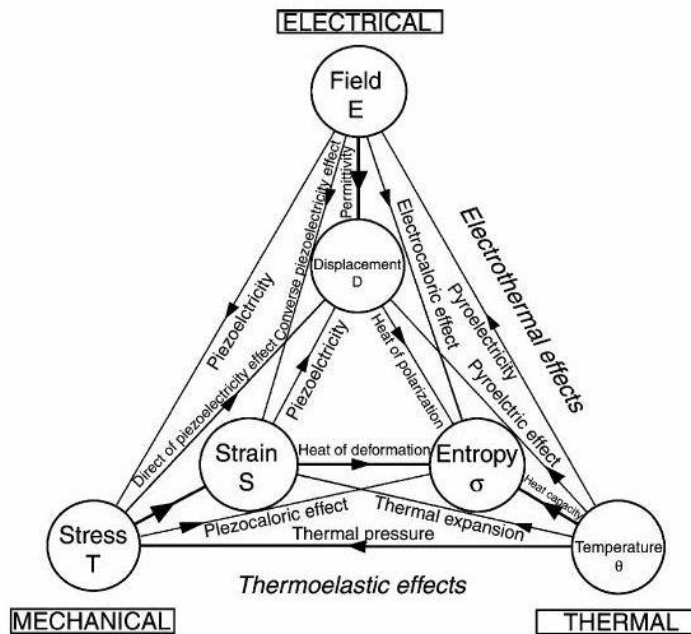


Figure 1.1 Heckmann and Thurston Diagram showing the electro-thermo-mechanical relations in a crystal, where T, S, E, D, θ and σ are stress, strain, electric field, electric displacement, temperature and entropy respectively. [2]

1.2.1 Piezoelectric Materials

Materials that generate an electric field due to mechanical deformation or conversely experience strain when subjected to an electric field are known as piezoelectric materials. The piezoelectric effect was discovered by Jaques and Pierre Curie in 1880 using multiple experiments with quartz crystals.

The transduction is due to the change in their crystal structure and their state of polarization. The molecular dipoles are either in a polarized state or a non-polarized state within the material. When an electric field is applied, they are forced to reorganize and align themselves in the direction of the field thus leading to permissible strain. This is known as electrostriction or converse piezoelectric effect.

The inversion of the stimulus induced transduction as well. The molecules generate an electric field when they are reoriented due to physical pressure which is known as piezoelectric effect. Though a lot of naturally occurring crystals such as Rochelle salt, Topaz, Quartz, Berlinite display piezoelectric effect, the material most used for this application is PZT – Lead Zirconium Titanate which is a ceramic Perovskite material of various shapes and sizes (as needed for application) shown in Figure 1.2. It is the most commonly used piezoelectric smart material because of deformation characteristics and the generated electric field. These smart materials are used in various applications such as structural health monitoring [3], energy harvesting, flow-control and micro-robotic applications.

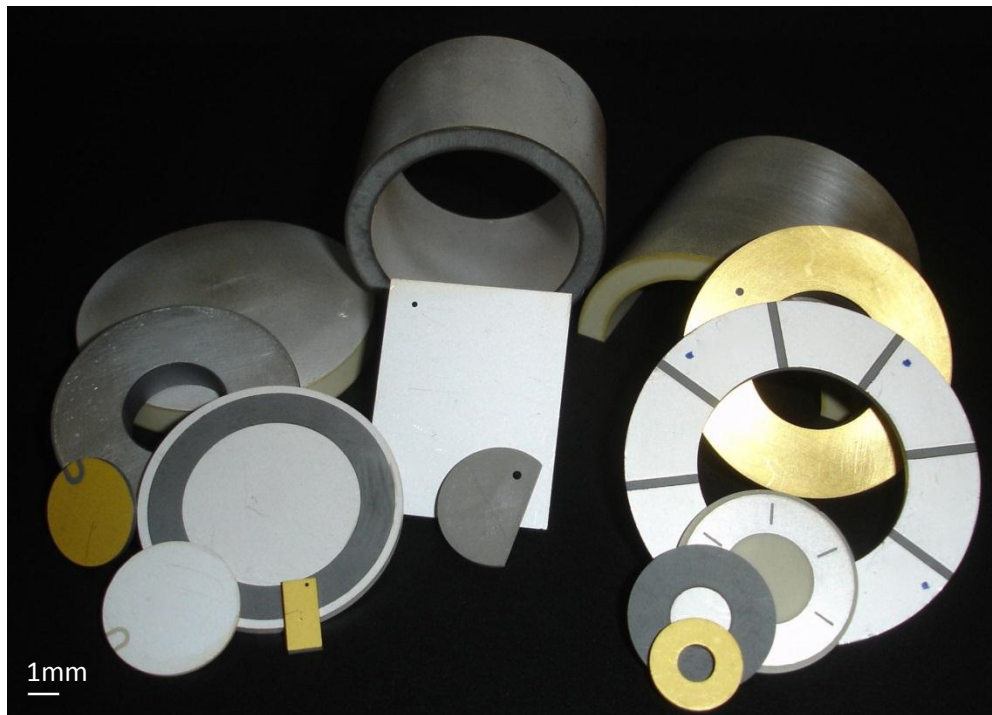


Figure 1.2 Different PZT shapes and sizes. [4]

1.2.2 Electro Rheological and Magneto Rheological Materials

Materials that display a change in their rheological properties (i.e. change in their viscosity thereby changing from a liquid to quasi solid state due to the application of an electric or a magnetic field) are known as electro rheological or magneto rheological materials. These are usually non Newtonian fluids and are generally called ER or MR fluids for brevity.

They are made up of fluids that are dispersed with either electrically active or magnetically active solid particles. These during the application of an electric field or a magnetic field, align themselves in the field direction thereby inducing a change in the viscous property. Figure 1.3 shows MR Fluid displaying change in viscosity under magnetic field.

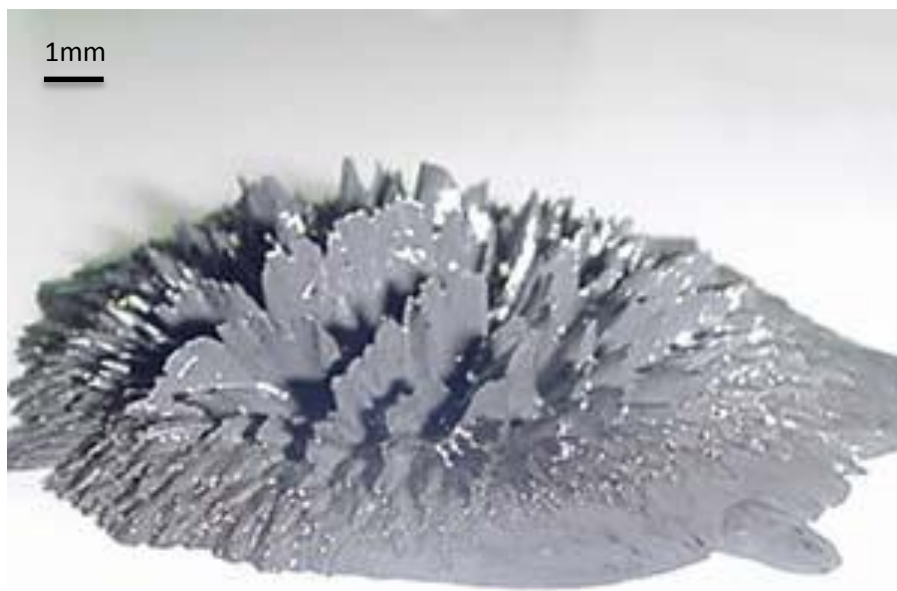


Figure 1.3 MR Fluid showing change in viscosity under applied magnetic field. [5]

These ER and MR Fluids are used in various applications in aerospace and mechanical engineering fields. They are used in automobile suspensions, in innovative space craft slosh damping systems and in smart clutch systems by various industries [1].

1.2.3 Shape Memory Alloys

Shape memory alloys are those which display a change in their microstructure due to a temperature stimulus thus effectively displaying what is known as “thermoelectric martensitic transformation” that results in shape change on a macro level as shown in Figure 1.4 of a spring being deformed and brought back to shape using temperature variation. The shape memory property was discovered as early as 1932 and has been worked upon extensively since then.

The most common shape memory alloy is the Nitinol or nickel titanium (the “noI” stands for naval ordinance laboratory where the properties were discovered). Other shape memory alloys are FeMnSi, CuZnAl and such which display relatively smaller shape memory effect compared to Nitinol. These shape memory alloys are known to “remember” their shape even after deformation since they possess a strong austenitic and a soft martensitic structure at high and low temperatures respectively. The phase change in the microstructure from martensitic to austenite state occurs by increase in temperature and when the temperature is lowered, the material returns back to martensitic state.

They are used in various applications such as de-icing, in control surfaces in aircrafts as well as in engines to reduce engine noise. They are used in car seats, climbing robots and also in everyday gadgetry such as lamp holders. They are one the most widely used smart materials in the industry. Their major disadvantage lies in the fact that they can be heated quickly but the cooling mechanisms tend to be slightly slower.

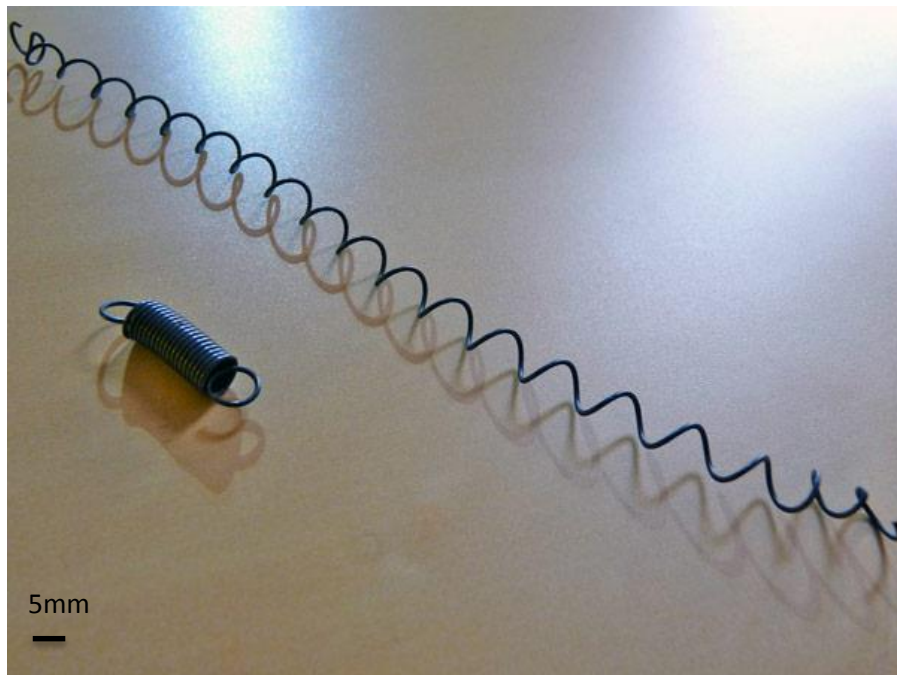


Figure 1.4 Shape memory alloy spring remembering its shape after deformation and heating. [6]

1.2.4 Chromic Materials

Chromic materials are those which change their color due to an external stimulus. This stimulus might be electrical in which case the material is known as electrochromic or due to variation in temperature which would term the material thermochromic or even change in the pH of the system which is called Halo chromic.

There are various types of chromic materials that are classified based on the external stimulus that affects the change in the color of the material. Some of them have been listed in Table 1.1.

Table 1.1 Chromic phenomena and their stimulus.

Phenomena	Stimulus / Caused by
Electrochromism	Electric field
Thermochromism	Temperature change
Photochromic	Light intensity
Piezochromism	Mechanical pressure
Halochromism	pH level
Tribochromism	Friction
Cathodochromism	Electron beam
Solvatochromism	Solvent polarity
Crystallochromism	Change in crystal structure

1.2.4 Polymer Based Smart Materials

Polymer based smart materials are mostly known as soft actuators and sensors because of the nature of actuation as well as their material properties. They may display various actuation phenomenon and not all the polymer based actuation principles are completely understood [7]. The actuation and sensing properties vary with the monomeric chains or the mode of actuation or the frequency and duration of the provided stimulus.

Though their uneven and sometimes unpredictable behavior seems unfavorable, it has to be understood that the reason behind this is because of the existence of multiple variables that impact their properties. Right from the manufacturing process to the electrode layers to the ionic content (in case of ionic polymers) within the polymers, everything can be varied and each variation causes a dramatic change. This allows for the possibility of tailor making customized properties for the actuator or sensor usage.

Looking at the various types of polymer actuators that are widely used, there are conductive polymers that show swelling due to an electric field or potential developed because of either an oxidation or a reduction process occurring within the system. These are usually biologically compatible and induce relatively large force with a small drive voltage [7].

Though they are slow when it comes to response time and have a low actuation frequency window, the most significant disadvantage is the fatigue they suffer from after a few cycles. Their performance decreases and effectiveness is reduced exponentially after long use. Some examples of conductive polymers are Polythiophenes, Polyanilines, Polypyrroles etc... [7,8].

Certain polymers such as Styrene acrylate and Cyanate ester display shape memory effect. When the temperature of the system is varied, the polymer chains undergo a morphology change that results in the shape change [8].

Though they display high strains and are extremely easy to manufacture, the down side to them is that they lack significant actuation speed and blocking force. They have very simple actuation mechanisms and respond well to temperature change when manufactured and tailored for particular applications [8]. But the customization of these

actuators and the manufacturing process itself needs to undergo rather huge changes to make these actuators commercially efficient for use.

Apart from these the other major kinds of polymeric actuators are called electro active polymers. They are not conductive as such but can show actuation properties when coated with electrodes and when an electric field is applied as a stimulus. These electro active polymers actuate very similar to natural muscles and hence are called as “artificial muscles”. This being said, their application in biomimetic robotics field is far reaching and they are being tested for used in all sorts of applications such as morphing wings wherein an airplane can have an avian - style flight to creating biocompatible prosthesis for amputees [7,8]. The impact of their use and their properties make them extremely useful for these applications and hence it can be safely said that they are among the most sought after smart materials technology on earth.

Electro active polymers or EAPs as they are called are still subdivided into two major classes that include electronic EAPs and ionic EAPs. Coulomb forces drive electronic EAPs. This means they are categorized according to the type of force that exactly determines their actuation behavior. They can be ferroelectric polymers, in which case they display non – centro-symmetric shape change behavior in the presence of an applied electric field as in the case of materials such as polyvinylidene fluoride-co-trifluoroethylene or P (VDF-TrFE).

They can also be piezoelectric polymers or electrostatic or electrostrictive or even dielectric elastomer polymers that require high drive voltage. Since they are electronically driven, they have good controllability and their actuation or deformation can be predicted. They also have a high energy density compared to other types of

polymer actuators but suffer greatly in their strength and reliability. The very high drive voltage also serves as a major disadvantage when considering applicability in real life.

The other Category of EAPs is the ionic EAPs class. These polymer actuators are driven by the mobility or diffusion of ions within the polymer membrane. They require very small drive voltage and do not have good energy density. And despite their poor controllability, they are preferred over other EAPs due to the fact that they give a large bending deformation under very small-applied electric potential.

The studies on EAPs have been gaining increased popularity lately due to the fact that the complete model of their working behavior has not been detailed yet on a micro scale and there is a major scope for it to be improved. They vary in their properties with very small changes in their electrode morphology or their ionic content and they are customizable according to the applied environment. They tend to function on the similar lines of natural muscles, closer than other EAPs and they can be manufactured to be biocompatible as well.

This research will discuss in detail about developing an enhanced ionic polymer metal composite actuator with focus on analyzing its electrode morphology and electromechanical properties. A physics based modeling of the same will also be discussed in the following sections.

CHAPTER 2 Ionic Polymer Metal Composites

Among smart materials the Ionic Polymer Metal Composites or IPMCs as they are most commonly referred to as are smart actuator sensors that produce a large bending deformation when they are subjected to a very small electric field [8]. Ionic polymer metal composites are a type of smart materials that fall under the category of ionic electro active polymers. They are electro active because they respond to an electrical voltage. They are made up of polymer membranes and since their actuation is through the movement of ions being either vehicular or structural, meaning either by the diffusion of protons or transfer of these protons between the clusters that they form, within the polymer membrane, they are given the term 'ionic' polymers. The actuation principle behind ionic polymer metal composites depends on fixed anions and mobile cations within these polymer membranes.

The polymer membrane absorbs water due to its porosity and displays swelling. The cations infused within the polymer membrane gets surrounded by these water molecules [9]. During the application of an external electric field on the electrodes of the IPMC, the mobile cations within the polymer membrane are displaced and there is a significant change in the mass flux due to this movement. This fluid influx towards one electrode causes a bending deformation on one side which is called the actuation mode of IPMC as shown in Figure 2.1.

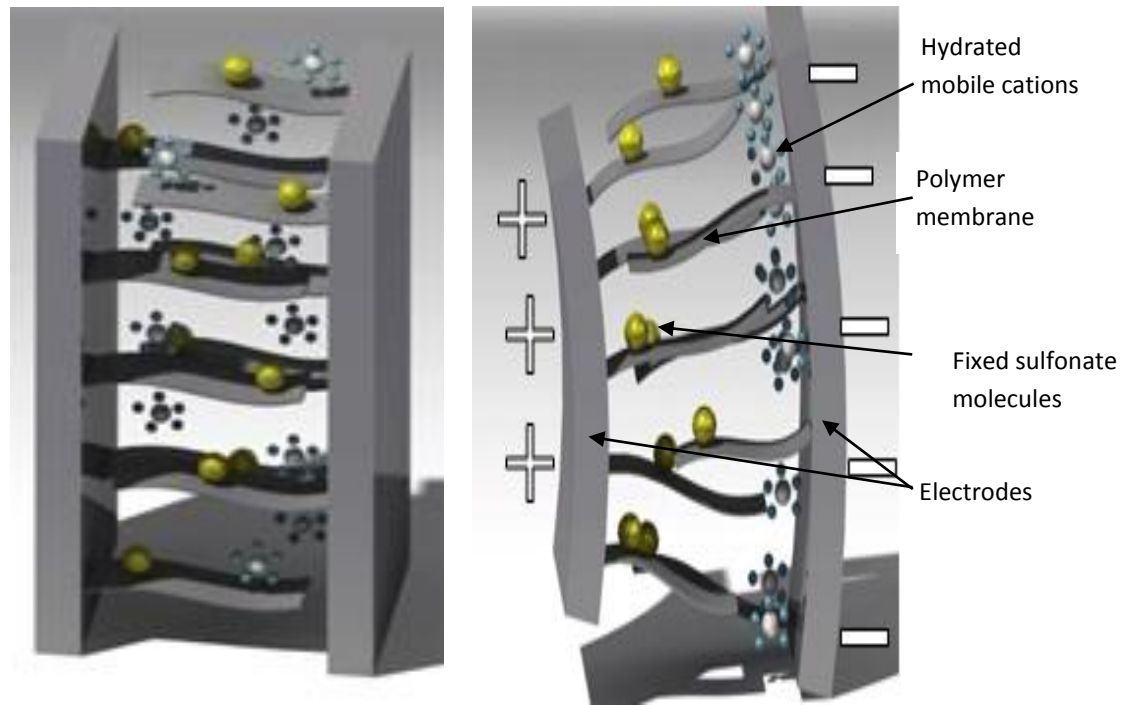


Figure 2.1 (a) IPMC before actuation (b) In presence of an electric field.

2.1 Polymer Membrane

To understand IPMC, the first step is the understanding of the polymer membrane that makes up the IPMC. The polymer membrane is the main component of the IPMC that deforms. There are various types of membranes used. Nafion (DuPont - USA), Aciplex (Asahi-Kasei – Japan), Flemion (AGC chemicals – Thailand), Hyflon (Solvay plastics – USA) are some of the membranes commonly used as ionic polymers for the actuators [10,11]. Significant research literatures and commercial availability of the product have propelled the use of Nafion as the ionic polymer material in this dissertation. Though structurally these membranes are very similar (all being perfluorinated proton transfer membranes) and the mechanisms involving the proton

transport within the membranes and the transport properties show significant similarities as well.

Nafion is a DuPont co-polymer which is used majorly in fuel cells as an ion exchange membrane. It is a copolymer of tetrafluoroethylene and perfluoro-3, 6-dioxa-4-methyl-7-octene-sulphonic acid. From light scattering experiments it has been proposed that the Nafion polymer has particles in the form of ribbon shaped elongated structure. They have been proposed to have a semi-crystalline matrix that contains ionic clusters within them. The morphology of this Nafion ionomer model was described as spherically shaped ionic clusters that have an inverted micelle structure.

The membrane is called a perfluorinated sulphonate because it has a pendant sulphonic acid group. This SO_3H group dissociates to give a SO_3^- after the proton release and hence is called as a sulphonate. The Nafion membranes are usually named as 117, 112, and 115 etc., in which the first two numbers denote the equivalent weight in hundreds and the last number denotes the thickness in one hundredths of an inch.

The equivalent weight or EW is given by the number of grams of dry Nafion per mole of sulphonic acid groups when the material is in acid form. Hence the Nafion 117 used in the project would contain 1100 EW and 0.007 in. or 0.1778 mm thickness.

The Nafion membrane thickness depends on the deformation and blocking force requirements of the IPMC application [12]. The thickness of the membrane affects the blocking force directly and affects inversely the deformation. Hence, for larger deformations, thinner Nafion membranes are used and for applications requiring higher blocking force, thicker Nafion membranes are used. It has to be noted that the electrodes on both sides of the Nafion membrane must be insulated by the membrane in itself [12].

Thinner IPMC models tend to have thinner edges that cause the electrodes from the top and bottom to smear into each other and create a short thereby slowing down the IPMC actuation or bringing it to zero because of the short. Hence an optimum size of 0.1778 mm was decided for this thesis.

The structure of the polymer is effective in a way such that when the sulphonic acid group undergoes dissociation [12], the proton released is allowed movement through the membrane. The fixed anions are deterred from any motion whatsoever within the membrane.

These membranes are highly corrosion resistant and can resist very high levels of chemical attack. They also have a very high operating temperature (limited by hydration and loss of strength) and can act as super acid catalysts because of the presence of their sulphonic acid group [11,12] .

Fluorocarbon backbone chains that add the strength and resilience to the polymer membrane repel hydrophilic sulphonate groups since they themselves are hydrophobic and this makes the sulphonate groups cluster together.

Studies by Gireke et al. [13] were done on the number of sulphonate sites per cluster and have also related them to the number of water molecules per cluster. They have shown that the water molecules per cluster increased with the water content in the perfluorinated membrane. They have also shown that these clusters increased on a linear trend.

The Gierke model also known as the cluster network model shown in Figure 2.2 explains the Nafion polymer membrane structure to a large extent. This model has been adopted by many literatures and has been found to be consistent with the results obtained during experimental validation.

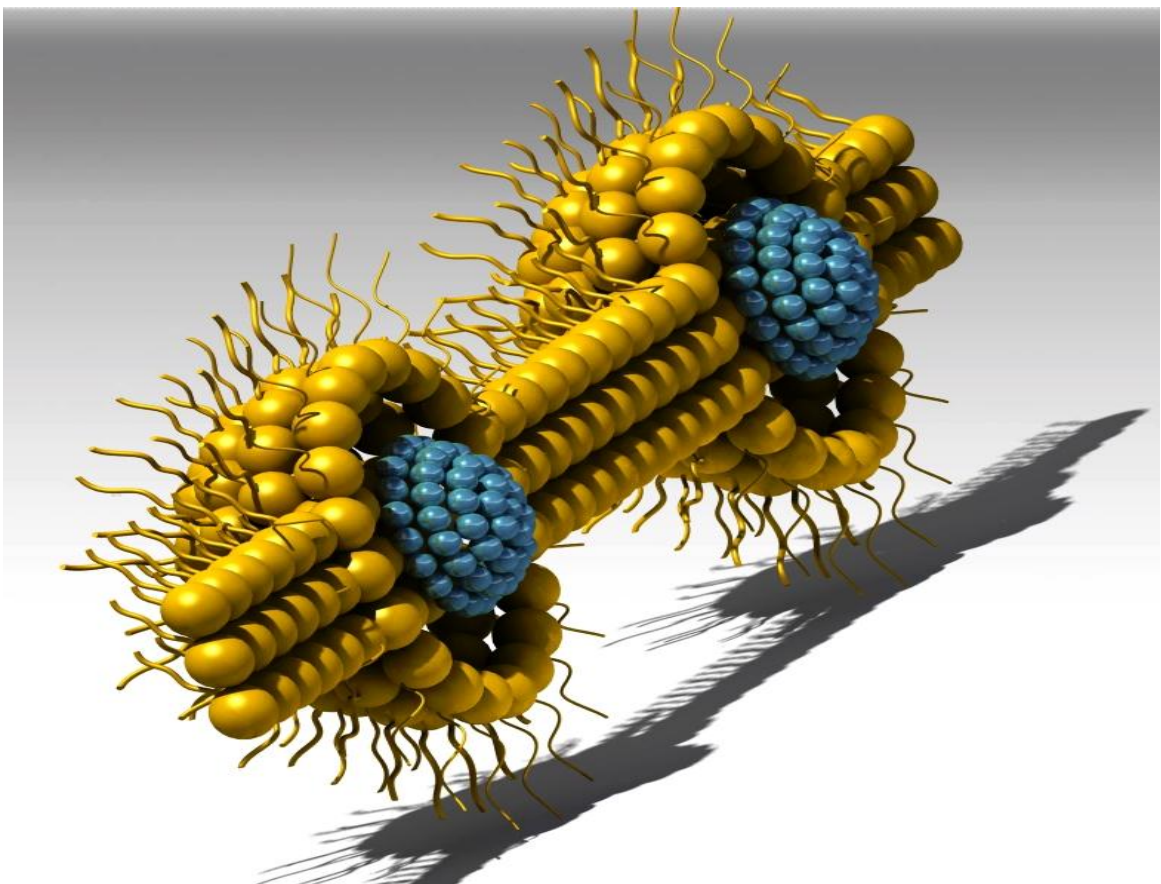


Figure 2.2 3-Dimensional rendering of Cluster-network model [13] for the morphology of hydrated Nafion. The SO_3^- ions are shown in yellow (shown as inverted micelle) and the water molecules are shown in blue.

2.2 Electrodes and Manufacturing

2.2.1 Different Types of Electrodes and Plating

The only way to apply a potential difference across an IPMC is to coat it with electrode. The electrodes on the actuator not only affect their stiffness and current properties but also would affect the actuation and robustness.

There are three types of electrode plating and three different methodologies that have been used in this thesis. The three types of plating used are

- 1) Electroless plating or chemical plating method
- 2) Direct assembly process
- 3) Sputter coating

Electroless plating or chemical plating method is used to plate platinum on to the surface of the polymer. This methodology causes the platinum electrodes to be chemically and electrostatically bonded to the Nafion membrane and ensures an extremely strong bond between the polymer membrane and the noble metal electrodes.

In the case of direct assembly process, the Bucky paper or carbon nanotube paper (multi-walled) electrodes are plated onto the surface of the membrane electrostatically and hence are stronger than sputter coated electrodes while still being weaker than the chemically plated electrodes.

In the sputter coating technique, gold electrodes are sputter coated on to the surface of the polymer membrane and are held onto it due to Van der Waals force and hence are weaker and have no directional characteristics compared to the other bonds.

They are short ranged as well and the advantage of using them is that they are temperature independent and do not get affected by the operating temperature [14].

2.3 Electroless Plating or Chemical Plating

The methodology used in this electroless / chemical plating technique was initially proposed by Keisuke Oguro et al. [14] and it has been used widely in IPMC research. It has to be noted that every single step in this plating process might affect the IPMC on a large extent when it comes to actuation. The initial pre-plating process involves roughening of surface of the polymer membrane to increase its surface area.

2.3.1 Mild Sandblasting and Ultrasonic Treatment

Sand blasting and ultrasonic treatment are the first preparations in treating a Nafion 117 surface before plating it. The sand blasting process makes sure that we obtain maximum surface area and treats the glassy surface of the polymer to a more evenly distributed surface for plating. As seen from Figure 2.3, the untreated surface shows mild glaze as well as uneven pitting that might have been caused by storage and handling. Sand blasting the surface roughens up the surface evenly.

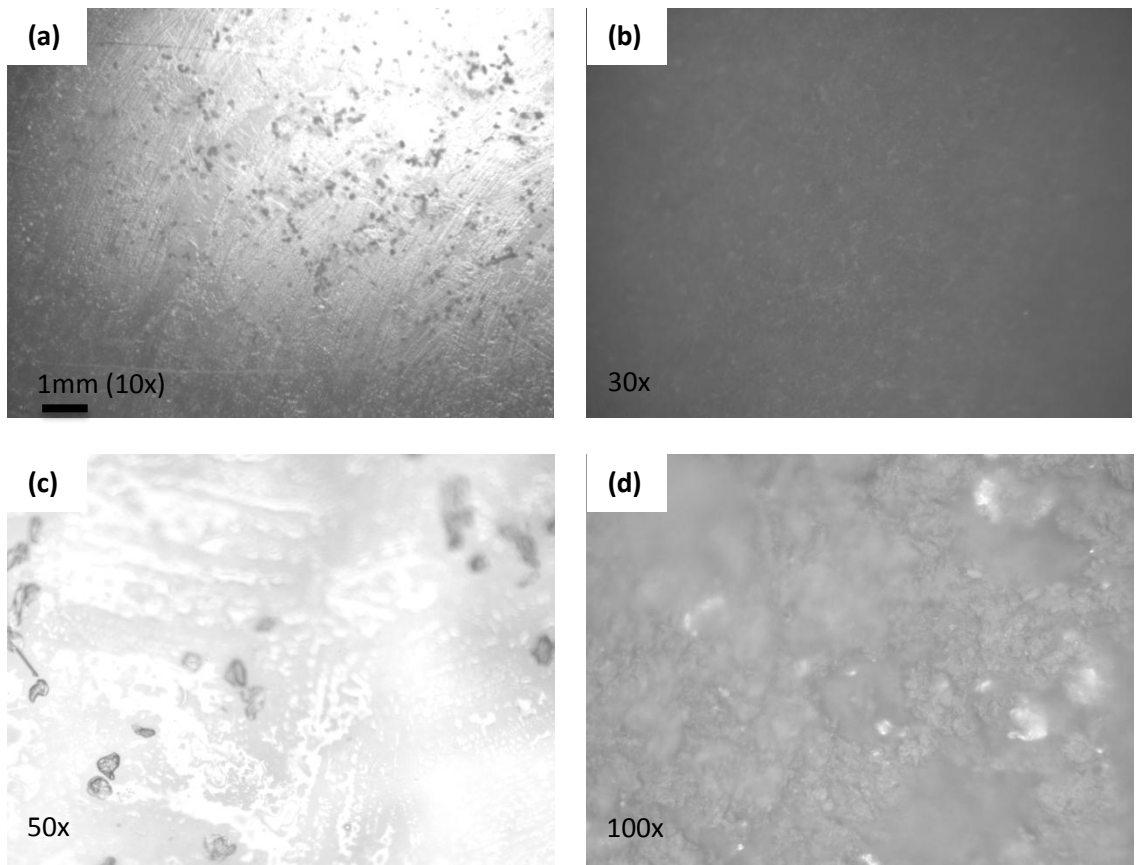


Figure 2.3 (a) Microscope image of Nafion 117 untreated surface (b) Microscope image of Nafion 117 sandblasted and ultrasonic washed surface showing uniform roughening (c) Untreated surface showing pitting and smoothness (d) Treated surface displaying increased surface area and uniform roughening.

Emery paper was also proposed to be used, though it created a more uneven roughening and this might cause uneven clustering of the ions which would further lead to uneven actuation. The pressure used was around 20-40 psi or 1.37 – 2.75 bar of compressed air blast using #80 sharp edge glass grit (Tacoma Company). Fine glass beads might be of better effect though literatures deem the difference marginal.

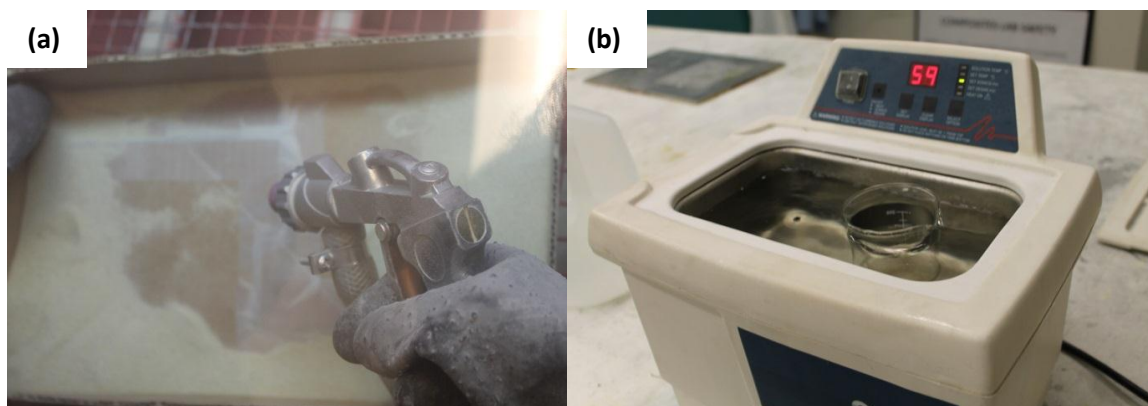


Figure 2.4 (a) Sand blasting (b) Ultrasonic cleaning.

Sandblasting is followed by ultrasonic washing shown in Figure 2.4. This process involves placing the roughened membrane in a Branson ultrasonic cleanser (CT, USA) in distilled water for around 2 hr. The temperature is maintained slightly above the room temperature and the cleanser is used at a frequency range of 30 kHz to 45 kHz. It passes ultrasonic waves through the operating area which causes millions of microscopic cavitation on the surface of the sandblasted polymer membrane to collapse which releases vast amounts of energy.

The bubbles released by the cavitation collapse during the process and this releases jets of water that impacts the surface to remove any dirt or particles sticking onto the membrane after sandblasting.

The surface is then treated with a 2N aqueous solution of hydrochloric acid. The membrane is placed in an Erlenmeyer flask within a fume hood and placed on a hotplate for 30 minutes. The acid boiling helps remove impurities and unwanted ions in the membrane as well due to environmental conditions or during the sandblasting and ultrasonic cleaning. Once the surface has been acid treated this way, it is again rinsed

with deionized water. The next step would involve swelling of the Nafion membrane using deionized water.

The structure of the sulphonic acid has a very high water of hydration. They can absorb 12 molecules of water for every sulphonic acid group contained within the polymer. The Nafion 117 membrane absorbs up to 22% by weight of water. When the membrane absorbs water, the clusters become smaller in number and larger in size. The membrane is boiled in deionized water for more than 30 minutes [14]. This process helps to remove the acid and swell the membrane and increases the water uptake [9,14]. Now the water swelled membrane can be stored in distilled or deionized water for further plating.

The plating processes that will be followed are of two major types. The process varies with variable use of the ionic solution to be used in the experiment along with change in the electrode type.

2.3.2 The Electroless Plating Method

The electroless plating is a pure chemical plating technique. In this thesis a fine layer of platinum is first reduced on to the surface of the membrane and later developed to form a thicker layer through continued reduction of the pure metal on to the surface. It involves three processes - the ion adsorption, the primary plating and the secondary plating [15].

2.3.3 Ion Adsorption

Ion adsorption process determines the amount of ions adsorbed on to the surface of the membrane for the plating purpose. Since it is a surface phenomenon, the previously sandblasted increased surface area helps more in this ion adsorption process.

A platinum complex Tetraammineplatinum (II) chloride hydrate ($[\text{Pt} (\text{NH}_3)_4] \text{Cl}_2 \cdot x\text{H}_2\text{O}$) salt is dissolved in distilled water to obtain a platinum salt solution. For the ion exchange process a 2 mg Pt/ml is required. The surface area of the polymer membrane determines how much of the solution is required. The ratio should be more than 3mg of platinum per cm^2 of the membrane area for effective adsorption.

It should be remembered that excess platinum solution only increases the adsorption as observed in the experimental procedures for this thesis and a 5% solution of ammonium hydroxide solution is further added for neutralization any residual acid from the boiling. This setup is allowed to stay for usually overnight or 24 hr or more depending on the membrane used and the adsorption rate. The more time the membrane stays in the solution, better results were obtained.

2.3.4 Primary Plating

Primary plating is a reduction process by which the platinum ions adsorbed on the surface of the membrane is reduced to form a fine layer of the electrode. The reducing agent used is a 5 wt % solution of aqueous sodium borohydride. It should be remembered

that this is a weight percentage and not a solution by volume or molarity. Hence 5 g of sodium borohydride is dissolved in 100 ml of water to obtain the solution.

The rinsed membrane is placed in stirring water bath at 40°C and 2 ml of the reducing agent is added every 30 min for approximately seven times while slowly increasing the temperature up to 60°C until the reagent is proportional to the area of the membrane. At the end of this process, 20 ml of sodium borohydride is added and stirred for an additional 1.5 hr at 60°C as shown in Figure 2.5 (a). At this point the fine deposits of platinum are obtained on the surface of the membrane and after rinsing with deionized water, it is immersed in dilute hydrochloric acid and allowed to stay for an additional couple of hours [14].

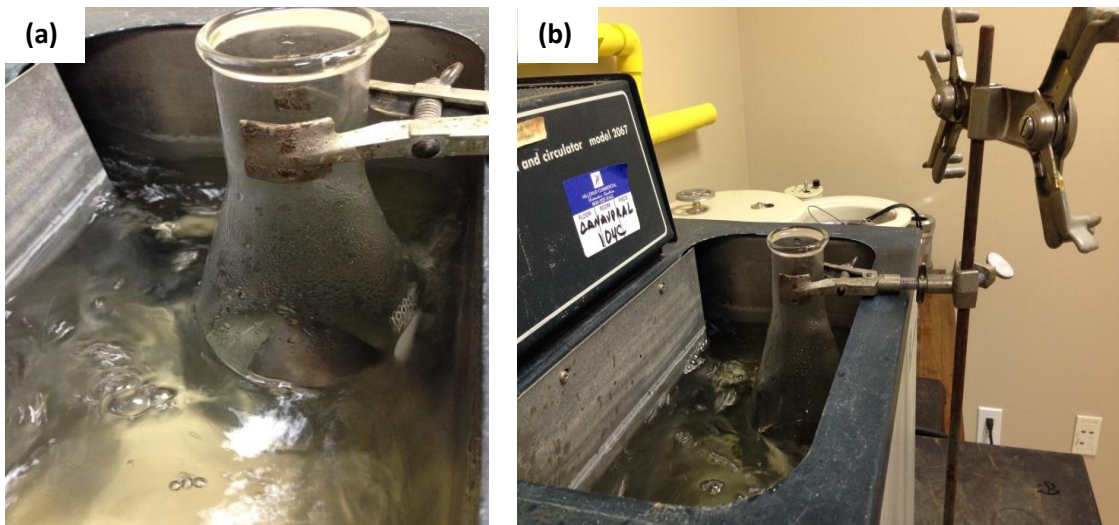


Figure 2.5 (a) Primary plating (b) Secondary reduction or development process.

2.3.5 Secondary Plating

This is the developing phase of the process wherein the fine layer of platinum on the surface of the membrane is developed to obtain a thicker layer of electrode. This plates an additional amount of platinum on the surface. A solution containing 2 mg/cm² of the membrane that is to be plated, is prepared from the platinum ammine complex. Hence the amount of solution directly depends on the polymer membrane area.

The amount of platinum in the solution directly affects the platinum amount that will be plated. Hence the more amount of platinum in the solution is desirable. The membrane is immersed in this solution and 5 ml of 5% ammonium hydroxide solution is added to it. A 5% aqueous solution of hydroxylamine hydrochloride (NH₂OH-HCl) and a 20% solution of hydrazine (NH₂NH₂) is prepared and kept aside to be used for the process.

The membrane is placed in a stirring water bath at 40°C as seen in Figure 2.5 (b). 6ml of the hydroxylamine hydrochloride solution and 3 ml of hydrazine hydrate are added every 30 min while the temperature is slowly raised to 60°C. After 4 hr the platinum is seen to be plated on the surface. At the end of this process, a small sample of solution is heated to a boil with the sodium borohydride solution to check for the end point.

If there remains anymore Pt in the solution the addition of 6 ml of the hydroxylamine hydrochloride solution and 3ml of hydrazine hydrate is continued until no black coloration is seen. Care should be taken not to add sodium borohydride to a hot solution since it might result in a gas explosion.

Once the plating process is complete, the plated membrane is rinsed in deionized water, and boiled with dilute hydrochloric acid (0.1 N) which removes the ammonium cations that have impregnated the membrane in the process of plating. This membrane is further immersed in a solution of a sodium/lithium chloride salt to replace the cations in them respectively.

2.4 Direct Assembly Process

Replacing the electrode from metal electrodes to a thin sheet of carbon nanotube known as Bucky paper, a direct assembly process is used. These Bucky papers have very high conductivity and variable porosity ratio allows for the ability of Bucky papers to be used effectively in IPMC research.

We know from theory that proton dissociation in the Nafion polymer membrane in the sulphonic groups yields us the sulphonate and H^+ ions. These ions are the highest contributors in the actuation though not as effective in terms of performance of an Ionic polymer metal composite. But they can be effectively replaced by sodium Na^+ , lithium Li^+ or imidazolium ions to enhance the actuation properties of the IPMC.

Before the ion replacement takes place, a few preliminary steps are undertaken to make sure that the ion replacement proves to be effective. A schematic of the entire process is shown in Figure 2.6.

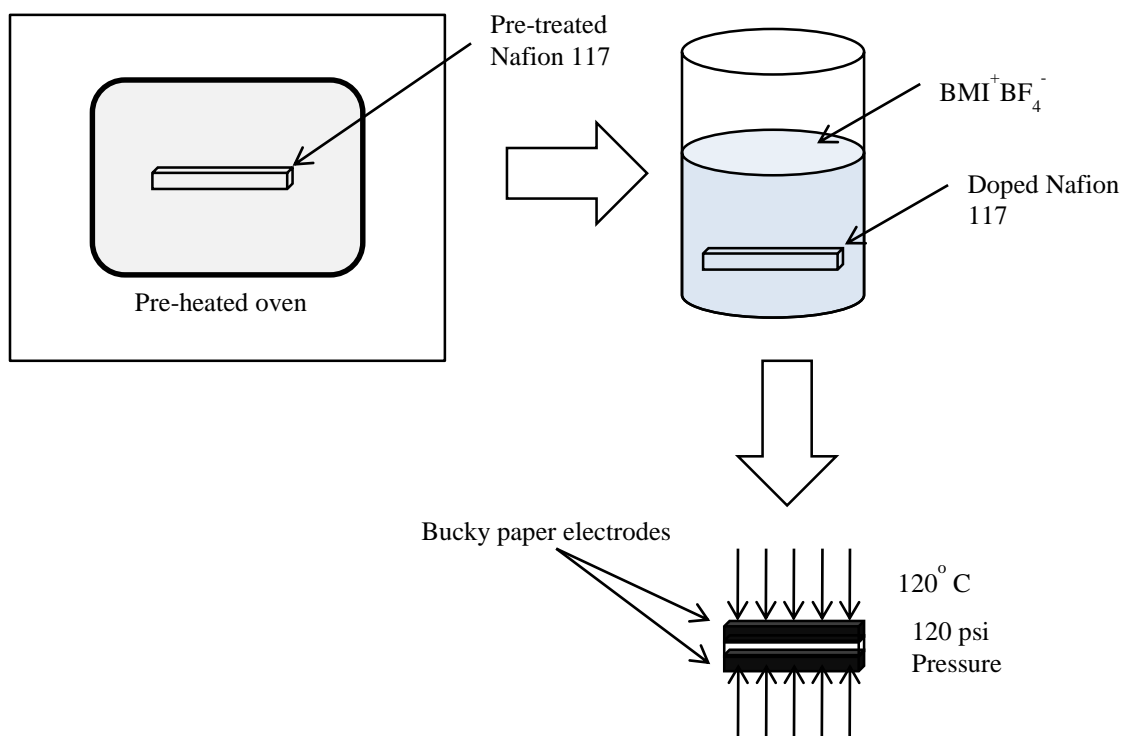


Figure 2.6 Direct Assembly Process schematic.

2.4.1 Vacuum Treatment

The polymer membrane after sandblasting and ultrasonic washing is boiled in dilute hydrochloric acid and rinsed with deionized water again. Then it is allowed to sit in vacuum for three hours in the oven at 120°C. Initially the membrane was vacuum bagged and kept in the oven as shown in Figure 2.7 (a).

But since the method did not suffice to be efficient, a vacuum glass desiccator displayed in Figure 2.7 (b) was used with high temperature vacuum grease. This helped in removing the water molecules in the Nafion.

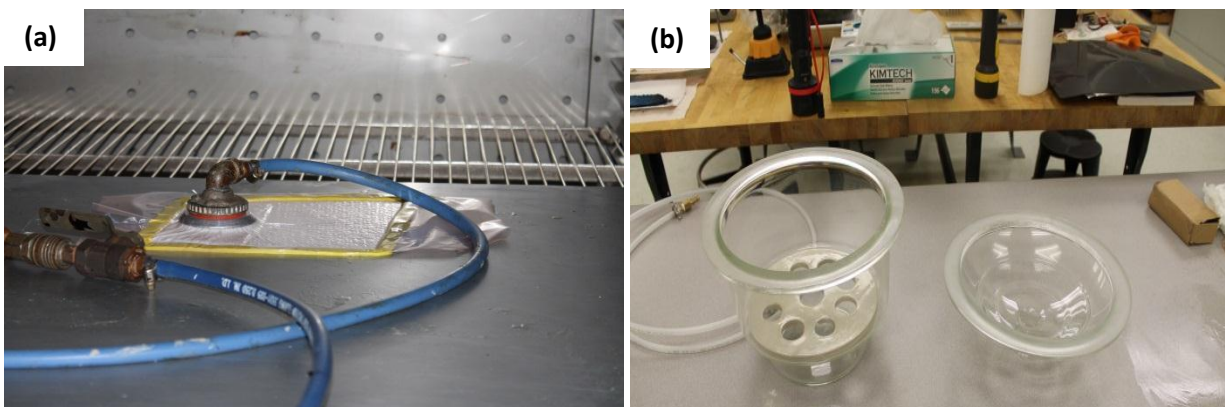


Figure 2.7 (a) Vacuum bagging (b) Vacuum desiccator.

2.4.2 Ion Replacement and Direct Assembly

After this process, the treated membrane is soaked in anhydrous solution of NaCl, LiCl and 1-butyl-3 methylimidazolium tetrafluoroborate (BMI+BF₄⁻) depending on the doping that is wished to be obtained as shown in Figure 2.8 (a). The now doped Nafion 117 membrane is sandwiched between the two Bucky paper layers and placed in hot pressed at 120°C at 120 psi for ten minutes as seen in Figure 2.8 (b)

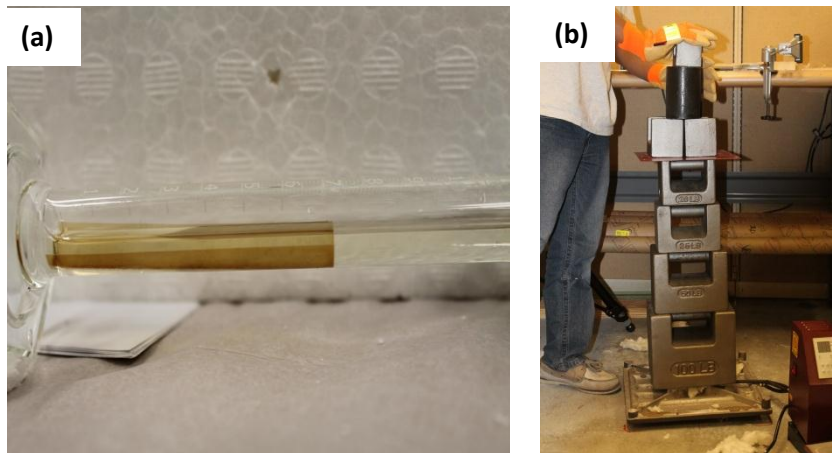


Figure 2.8 (a) Ion doping process (b) Manual heat press.

This sandwiched polymer membrane should be checked thoroughly for an even and a perfect fusion between the membrane and the Bucky paper in order for the field to be even on the polymer membrane and for charge transportation which in turn results in the motion of the ions from one side of the Nafion membrane to another to effectuate the actuation/bending deformation.

2.5 Sputter Coating

For testing another electrode, gold is sputter coated on top of the polymer membrane using a Cressington Scientific (Hertfordshire, UK) Sputter Coater. This covers the polymer membrane with a layer of gold that is deposited from a target. In sputter coating, a glow discharge is formed between electrodes by the means of a gas such as argon as seen from Figure 2.9.

Inside a vacuum chamber, an inert gas (argon) is passed. Here electrons and free-ions get attracted to the respective oppositely charged electrodes and a small electric current is generated. This electric current when increased causes the potential to cross the breakdown potential because of the collision of electrons and the inert gas (argon in this case) ions. This causes a self-sustaining glow discharge. When this glow discharge between the cathode and the anode occurs, the cathode is bombarded with the heavy gas ions. This causes the cathode to be eroded. This is called as plasma sputtering. This causes an omni-directional deposition of the cathode material or the “sputter atoms” on to the sample and the work chamber.



Figure 2.9 Sputter coating process.

2.5.1 Sample Preparation

The sample is prepared by sandblasting and ultrasonically cleaning it with distilled water. It is then checked and mounted on a suitable stub for use on the coater sample table. The sample is dried thoroughly before mounting and made sure it lies within the conducting path during the sputter coating process.

2.5.2 Table Height

The sample table height in the coater is adjusted to make it suitable for the sample. It is initially set to 35 mm which provides an optimal distance from the target and assures that the conductive path covers the entire sample. The sample is then placed on the table and the top plate is closed.

2.5.3 Sputter Settings

The chamber is closed and checked for the seals. The gas control knob is initially ensured to be in the closed position and the sputter coater output power control is set to give maximum power.

2.5.4 Cylinder and Regulator Settings

The argon gas cylinder is then opened and the regulator valve is adjusted to give a pressure of 0.3 bar. It has to be made sure that the pressure is to be increased slowly since there will still be line pressure in the system if the pressure limit is crossed over the shown value. Maintaining a constant pressure ensures that the sputter coating layer thickness will remain uniform. After the argon regulator pressure is set to 0.3 bar, the chamber is pumped with a chamber pressure lower than 0.05 mbar.

2.5.5 Timer and Sputter Coating

The timer is set to an initial value of 40 s. Increasing the time increases the amount of sputter coating layer. In this project, 4 layers and 8 layers of sputter coating samples are tested. For a more effective layup, the sputter coating is allowed to run for at least 40 s for each layer and the samples are coated for four and eight times to obtain the final layup. The gas control is set to obtain a chamber pressure with argon gas to more than 0.4 mbar and this is allowed to flush for at least 10 s.

After it is flushed, the gas control valve is adjusted to obtain a desired operating pressure of 0.08 mbar. The current is tested to give an initial value of 30 mA and the sputter coating process is started. The plasma glow is seen and sputter coating of the sample occurs. When the timer resets from 40 s to zero, it is again pressed once more for the second layup and the process is repeated until 4 or 8 layers of sputter coating is achieved as necessary.

The sample is then turned over and the entire process is repeated from the first as before. Each time sputter coating is done on one side of the sample, the gas control is closed and the system is turned off before venting the chamber. Once the chamber is vented, the top plate is lifted and the sample is moved out of the chamber before the next sample is placed or the sample is inverted and placed back.

It has to be made note that the sample will be cut along the edges to remove the electrode layer from the sides of the sample and hence the sample size will have to be larger than the desired size for the final test sample to allow for a buffer when the sample is cut.

2.5.6 Ion exchange

The final cut samples are allowed to soak in sodium chloride and lithium chloride for different samples to achieve the respective ion impregnation within Nafion and hydration of the polymer membrane to effectuate the actuation. It has to be made sure that the samples are handled extremely carefully because sputter coating might wipe off the sample surface when handled in a rough manner.

CHAPTER 3 Finite Element Method – COMSOL Modeling

The multiphysics model was built using COMSOL 4.4 multiphysics software. The main motive of modeling it on a multiphysics platform was to ensure that all the basic physics of the IPMC was captured in essence and that the base model acted in principle how a real life model would actuate. This being the aim, multiple modules of the software were used and coupled to generate a moderately accurate model of the polymer membrane actuator.

Since the model is slightly complicated, only platinum electrode IPMC has been modeled. The gold and Bucky paper IPMCs are slightly more complex taking into consideration the type of bonding between the electrodes and the membrane.

A 2 dimensional model of the IPMC was generated for the study since even on a two dimensional scale the physics behind the actuation remains complicated. The capacity of the software to apparently seamlessly integrate various modules allows the use of different physics behind each phenomenon that is witnessed on both macro and micro scales.

Three physics modules and four physics study interfaces are applied for the sake of this research and each module or interface is controlled and limited by variables fed into them from the previous module or interface. Since the output of one module or interface determines the input of another module or interface irrespective of the domains they are applied on, the base physics remains moderately real with feedback control between the interfaces.

The modules that are used in the study are

1. AC/DC module - Electric currents and the electrostatics interfaces
2. Batteries and fuel cells module - Transport of dilute species interface
3. Structural mechanics module - Solid mechanics interface

3.1 The Modules and Interfaces

3.1.1 The AC/DC Module

The AC/DC module is used because it can design, predict and analyze both static and dynamic electric and magnetic fields for low frequency applications. In this module, Maxwell's equations and its subsets are used for the modeled systems formulations.

These are combined along with material laws and solved to obtain partial differential equations that correspond to the initial conditions and the boundary conditions that are given to the model.

3.1.2 The Electric Current Interface

Like the name suggests, the electric current interface within the AC/DC module is used to solve for electric current flow both in capacitive as well as conductive cases. Equations of current conservation are solved in this interface to obtain values for the electric potential.

3.1.3 The Electrostatics Interface

The electrostatics interface is generally used for charge conservation in dielectrics and is predominantly used in static conditions. This interface solves for the above mentioned charge conservation equation. It is to be noted that this model is combined with other transport models (either for single species or multiple species) when it is used in transient condition which are found either in electrochemistry, chemical engineering or batteries and fuel cells module.

3.1.4 The Batteries and Fuel Cells Module

The batteries and fuel cells module deals with equations that solve for the electrolyte and electrode and other transport functions that occur within batteries and fuel cells. By changing different variables within the module the influence of various parameters affecting the system such as electro catalysts, pore distribution, electrolyte composition can be studied and understood.

It has to be understood that the equations solved for the system under the Batteries and fuel cells module would solve for conservation of current, charge, chemical species, and energy based on the initial and the boundary conditions that are given.

3.1.5 The Transport of Diluted Species Interface

The transport of diluted species interface exists within the chemical species transport interface in COMSOL. This interface deals with the diffusion, convection and as well as migration of chemical species within the system that happen due to an applied electric field. Here one of the components exists in excess compared to the other.

This interface solves for mass balance equation in order to obtain the distribution of concentration in a solution of a particular chemical species, considering diffusion, dispersion, convection, and chemical reactions.

3.2 Modeling

The above mentioned modules and interfaces are used in developing a model of IPMC that would track fluid interactions and concentration distribution of ions within the IPMC and try to link it to the displacement when an electric field is applied. The IPMC's polymer membrane is taken as a rectangle and meshed initially and tested for the above physics modules. Once a confirmation of the working was performed, the model was modified to include electrodes on both sides of the polymer membrane.

3.2.1 Geometry

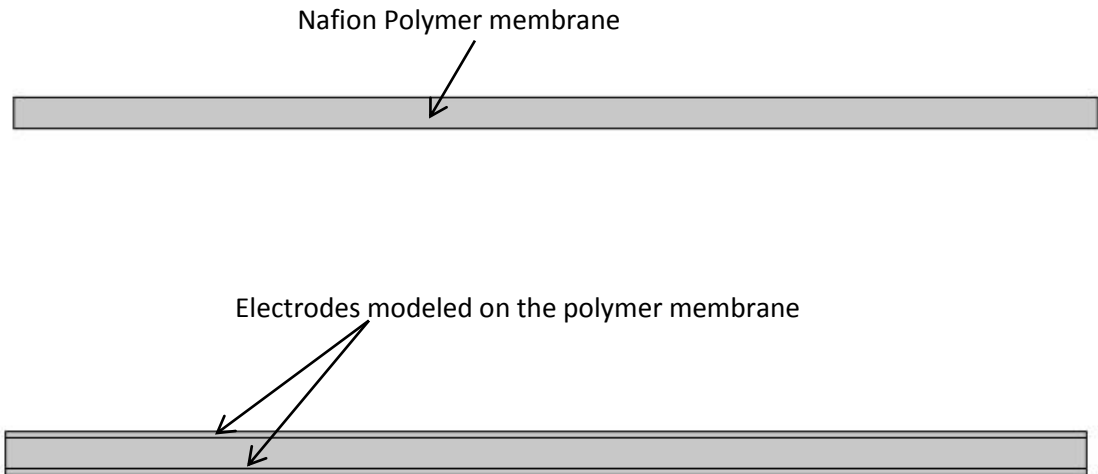


Figure 3.1 COMSOL geometry of membrane without and with electrodes.

As shown in Figure 3.1, the IPMC has been modeled in two different ways. First the membrane is modeled as a rectangle with high aspect ratio after which the electrodes are modeled. The center section is the Nafion domain whereas the outer rectangles are the electrode domains.

The IPMC is modeled as a water channel with ion movements within the solution. The anion mobility is made zero such that the entire body force is due to the displacement of the mass flux when the hydrated cations are transported across the channel.

The parameters and the variables initially declared for the model are provided below in Table 3.1 and Table 3.2.

Table 3.1 Parameters used in COMSOL model.

Name	Expression	Description
D1	$0.7 \cdot 10^{11} \text{ [m}^2/\text{s]}$	diffusion coefficient of cation
D2	$1 \cdot 10^{-9} \text{ [m}^2/\text{s]}$	diffusion coefficient of anion
T	300 [K]	temperature
c02	0.00 [mol/(m ³)]	upstream concentration of anion
c01	1200 [mol/(m ³)]	upstream concentration of cation
gasc	8.314 [J/K/mol]	gas constant
um1	$2.9 \cdot 10^{-15} \text{ [mol*s/kg]}$	mobility of cation
um2	0 [mol*s/kg]	mobility of anion
z1	1	valence of cation
z2	-1	valence of anion
eps	$.2 \cdot 10^{-1} \text{ [F/m]}$	dielectric permittivity
eps_0	$8.85 \cdot 10^{-12} \text{ [F/m]}$	dielectric constant in vacuum
V0	10 [V]	applied voltage drop
epsilon_nr	eps/eps_0	relative permittivity of water
rho	3105.5 [kg/m ³]	density of water
eta	$1 \cdot 10^{-3} \text{ [Pa*s]}$	viscosity of water
L	70 [mm]	channel length
H	2 [mm]	channel height
EH	0.4 [mm]	electrode height

Name	Expression	Description
Farad	96458 [C/mol]	Faraday's Constant

Table 3.2 Variables used in COMSOL model.

Name	Expression
space_charge	Farad*(c1 - c01)
alpha	.001 [N*m/mol]
beta	0.0055 [N*m^4/(mol^2)]
t	3 [s]
Fv	(alpha*space_charge) + (beta*((space_charge)^2))

3.2.2 Materials

The material properties for Nafion and the platinum electrodes were selected from the work of Benjamin Mead University of Nevada, Las Vegas [20]. These values proved to obtain consistent results when compared with experiments. The domain selection for the platinum domain is shown in Figure 3.2.

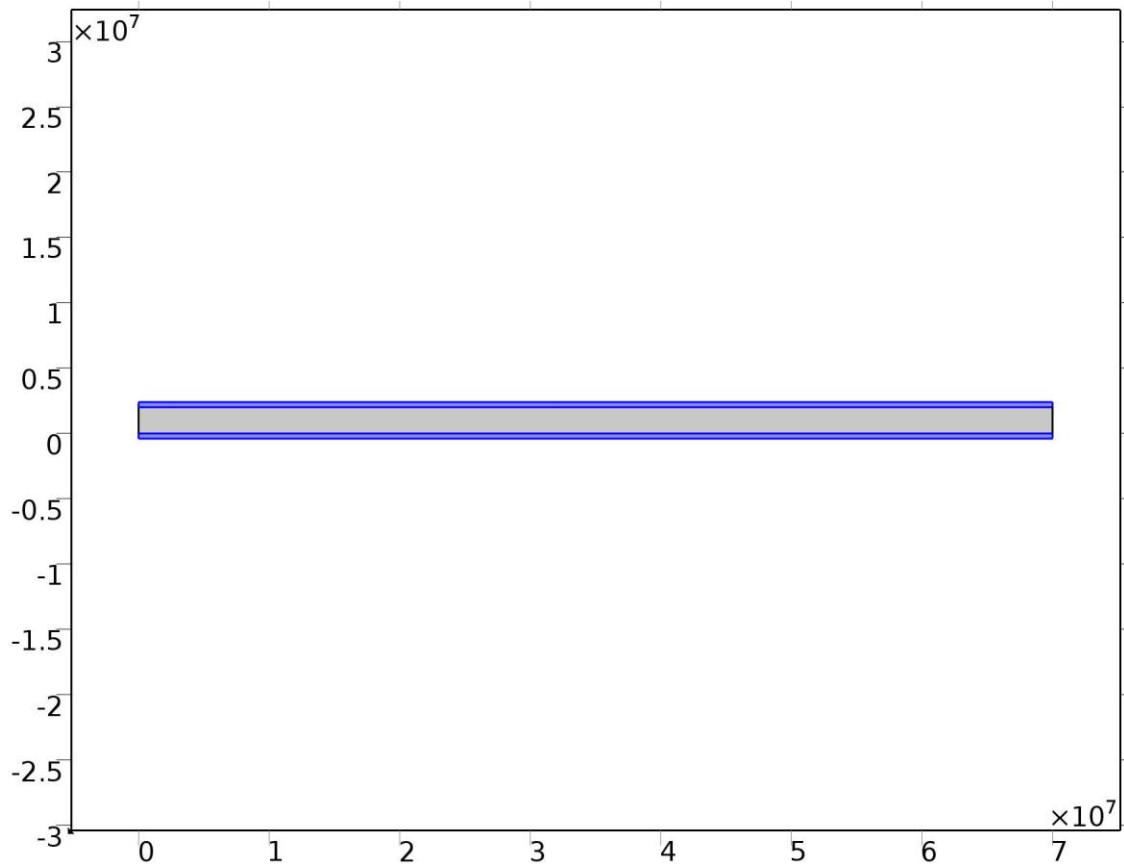


Figure 3.2 Platinum electrode domain selection (nm).

Table 3.3 and 3.4 give the Platinum material domain selection and the material properties for the selected domain. These will be used in the equations in Multiphysics.

Table 3.3 Platinum domain selection.

Geometric entity level	Domain
Selection	Domains 1, 3

Table 3.4 Platinum material selection.

Name	Value	Unit
Relative permittivity	eps/eps_0	1
Density	21450	kg/m ³
Poisson's ratio	0.38	1
Young's modulus	1.68*10 ⁺¹¹	Pa
Electrical conductivity	1.50*10 ⁺⁰⁴	S/m

Figure 3.3 gives the Nafion polymer membrane materials selection. It has to be taken note that the membrane's structural features such as its cluster network as not been modeled as such but the material properties in general alone are included.

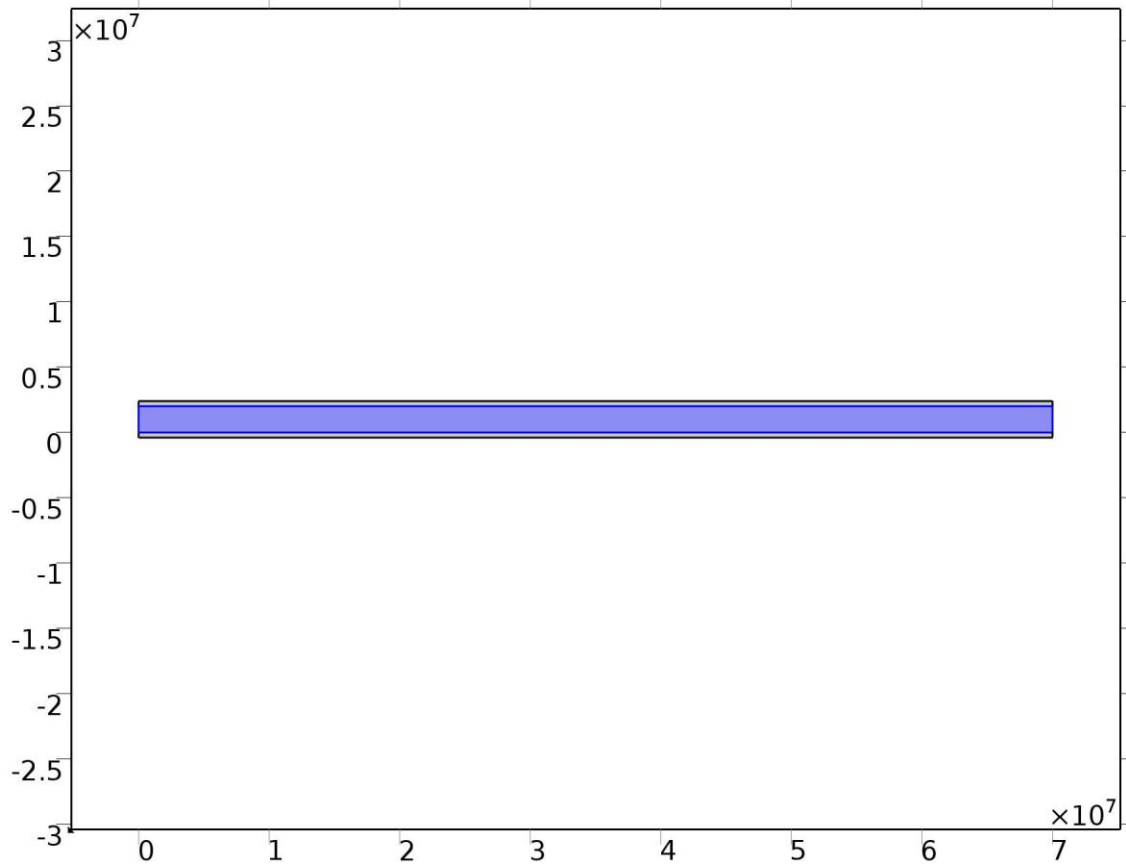


Figure 3.3 Nafion membrane domain selection (nm).

Table 3.5 and Table 3.6 give the Nafion polymer membrane material domain selection and the material properties for the selected domain. These will be used in the equations in Multiphysics.

Table 3.5 Nafion domain selection.

Geometric entity level	Domain
Selection	Domain 2

Table 3.6 Nafion material selection.

Name	Value	Unit
Young's modulus	$4.10 \cdot 10^{+07}$	Pa
Poisson's ratio	0.49	1
Density	3105.5	kg/m ³
Electrical conductivity	$5.00 \cdot 10^{+03}$	S/m
Relative permittivity	eps/eps_0	

3.3 Mesh

Because of the high aspect ratio of the model, a mapped mesh was developed to obtain acceptable accuracy of the model and still manage to keep the computation time reasonably fast. Since the problem involves migration, finer meshes were needed especially near the boundaries to resolve varying concentration. The detailed values for the mesh are given below in Table 3.7.

Table 3.7 Mesh details for the model.

Property	Value
Minimum element quality	0.5923
Average element quality	0.7834
Triangular elements	0
Quadrilateral elements	5453
Edge elements	1186
Vertex elements	8
Calibrate for	Fluid dynamics
Maximum element size	244000
Minimum element size	11200
Curvature factor	0.6
Maximum element growth rate	1.25
Predefined size	Coarser

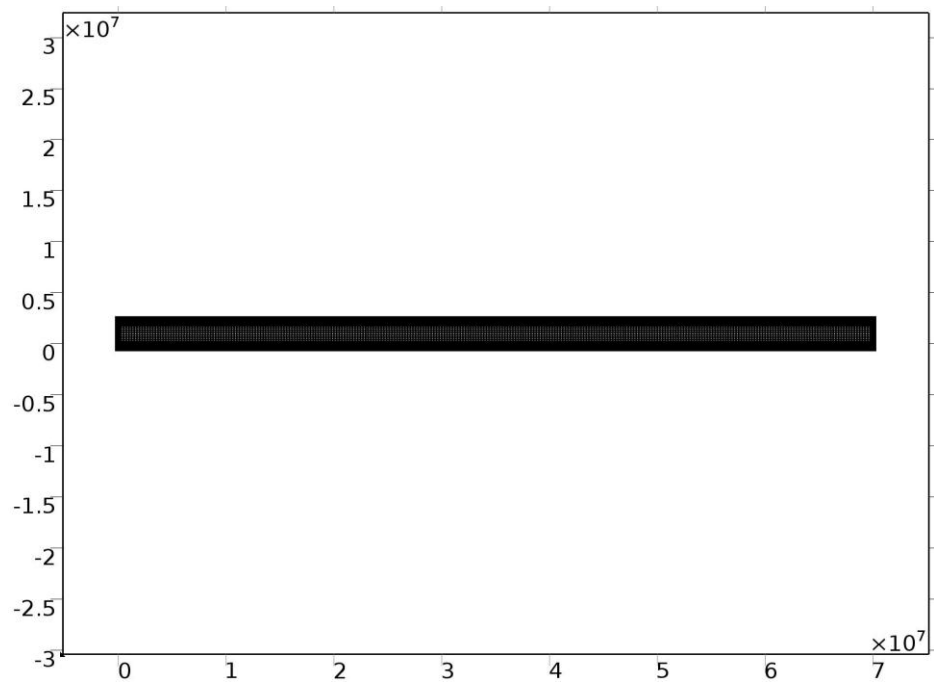


Figure 3.4 Full view of the dense mesh in COMSOL (nm).

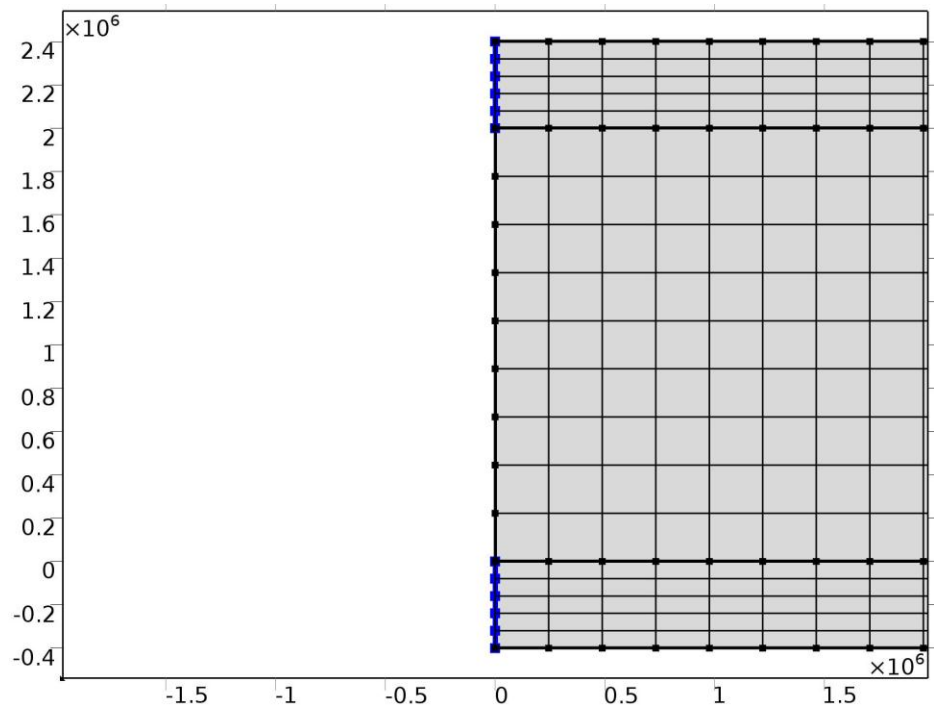


Figure 3.5 Enlarged view of the mapped meshing of the high aspect ratio element in COMSOL (nm).

It is to be noted from Figure 3.4 and Figure 3.5 that the mesh was generated on the domains keeping the higher resolution for the domains that are important for the analysis, while providing a less dense structured mesh for the remaining domains.

The mesh can be refined furthermore to obtain a more accurate result for the model but when really fine meshes are used, the deformation model breaks down.

3.4 Multiphysics

The first module used is the Electric currents module. This module solves for electric current flow in the electrodes as shown in Figure 3.6. Table 3.8 gives the selected domains.

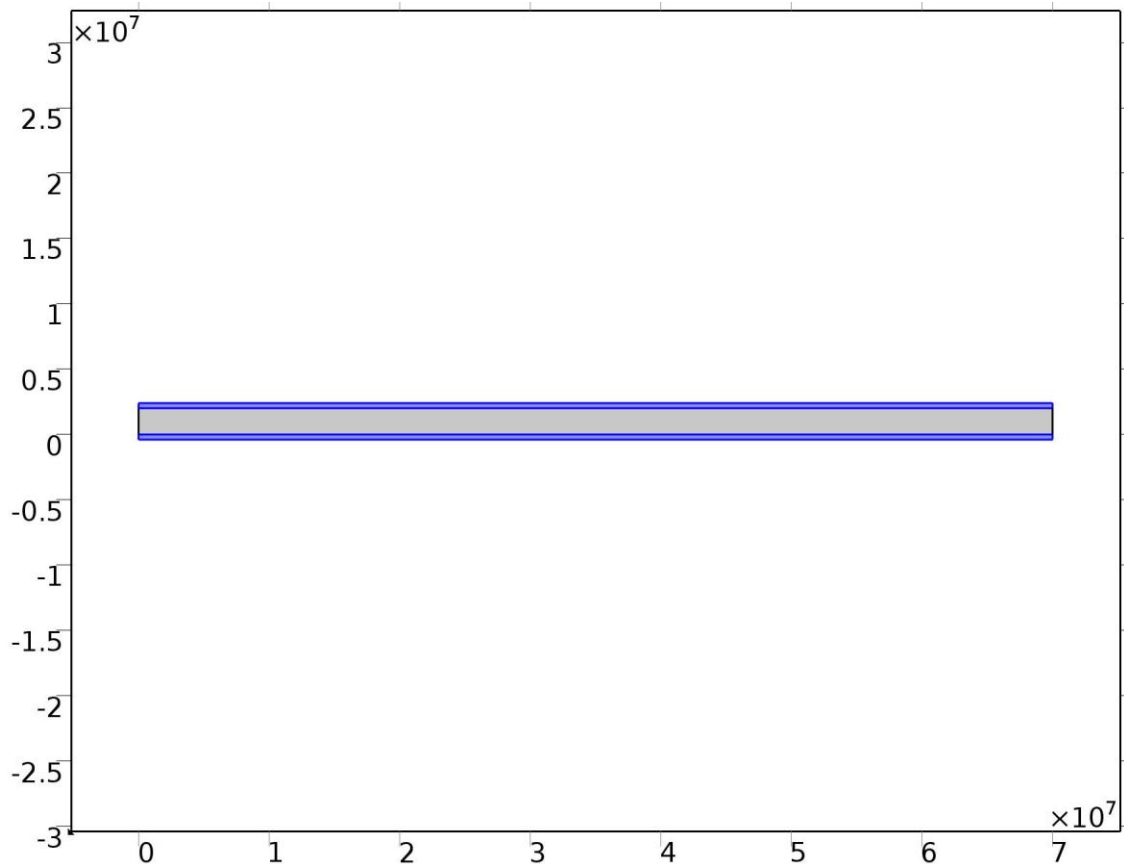


Figure 3.6 Electric current domain selection (nm).

Table 3.8 Electric current domain selection.

Geometric entity level	Domain
Selection	Domains 1, 3

Equations

The following equations are solved wherein, in the equation, the electric current is given by J , the electric field is given by E , σ is the materials conductivity and voltage field is V . The settings used for solving these equations are given in Table 3.9. The electric field is obtained through equation 3.

$$\nabla \cdot \mathbf{J} = Q_j \quad (1)$$

$$\mathbf{J} = \sigma \mathbf{E} + \mathbf{J}_e \quad (2)$$

$$\mathbf{E} = -\nabla V \quad (3)$$

Table 3.9 Electric current settings selection.

Description	Value
Electric potential	Quadratic
Value type when using splitting of complex variables	Complex

Description	Value
Frame	Spatial
Out-of-plane thickness	1
Activate terminal sweep	Off
Reference impedance	50 [ohm]
Parameter to export	Z

In this module the equations are solved for current conservation for the platinum electrode domains. Electric insulation layers between the electrodes and the polymer membrane are selected and the initial value for the electric potential on the electrodes is set to zero. One of the electrodes is grounded while the other electrode is assigned an electric potential of V_0 . It has to be taken note that V_0 is assigned a step function that makes it go from 0 volts to 10 V in a time step 't' that is assigned 3 s arbitrarily. This solves for only the electrodes. The electric field in the electrodes is then applied to the polymer membrane by the use of the electrostatics interface.

The electrostatics module is used to solve for the electric potential on the polymer domain. This is in effect with the electric field vector generated by the electrodes from the previous electric currents interface.

The high conductivity of the electrode material property applies the field directly onto the polymer domain, on the insulating interfacial boundaries. Figure 3.7 shows the electrostatics domain. Here the domain selection has been shown visually in the image and the entity level and selection are given in Table 3.10.

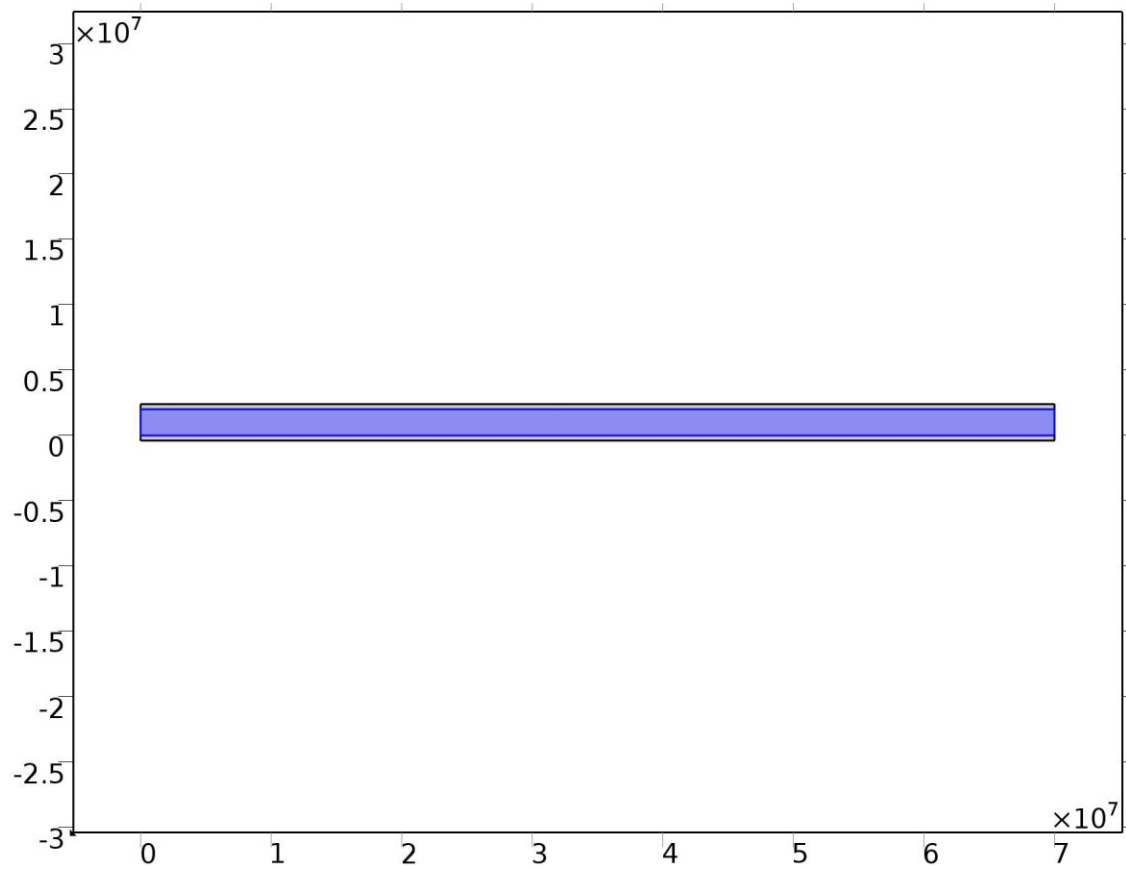


Figure 3.7 Electrostatics domain selection (nm).

Table 3.10 Electrostatics domain selection.

Geometric entity level	Domain
Selection	Domain 2

Equations

The displacement field \mathbf{D} and the electric field \mathbf{E} are equated to the charge density and voltage field V respectively. This electric field value over the polymer domain gives the value of the electric field to the next interface and hence is extremely important to be calculated properly. The interface settings are shown in Table 3.11.

$$\nabla \cdot \mathbf{D} = \rho_v \quad (4)$$

$$\mathbf{E} = -\nabla V \quad (5)$$

Table 3.11 Electrostatics settings selection.

Description	Value
Electric potential	Linear
Value type when using splitting of complex variables	Complex
Frame	Spatial
Out-of-plane thickness	1
Activate terminal sweep	Off
Reference impedance	50 [ohm]
Parameter to export	Z

The charge is conserved on the domain with zero charge on the interfacial boundaries of the domain. The initial value of the electric potential is set to zero and the space charge density is defined from the variable definition declared previously.

The space charge density initiates the mass transfer i.e. the migration of ions within the polymer membrane. The Transport of dilute species interface captures that accurately. The diffusion and migration region is set to the polymer domain with no flux condition in the interfacial boundaries.

The domain selection and entity level is given in Table 3.12 and visually given in Figure 3.8. The transport settings are given in Table 3.13. Here the flux specification of each species is done individually and the mass transfer coefficient is calculated by boundary layer theory. It is to be noted that in the no flux domain on the interfacial boundaries, no mass flows in or out. This is an important criterion to specify since there is no ion migration from the polymer to the electrodes and makes sure that it increases the accuracy of the model and does not break it down.

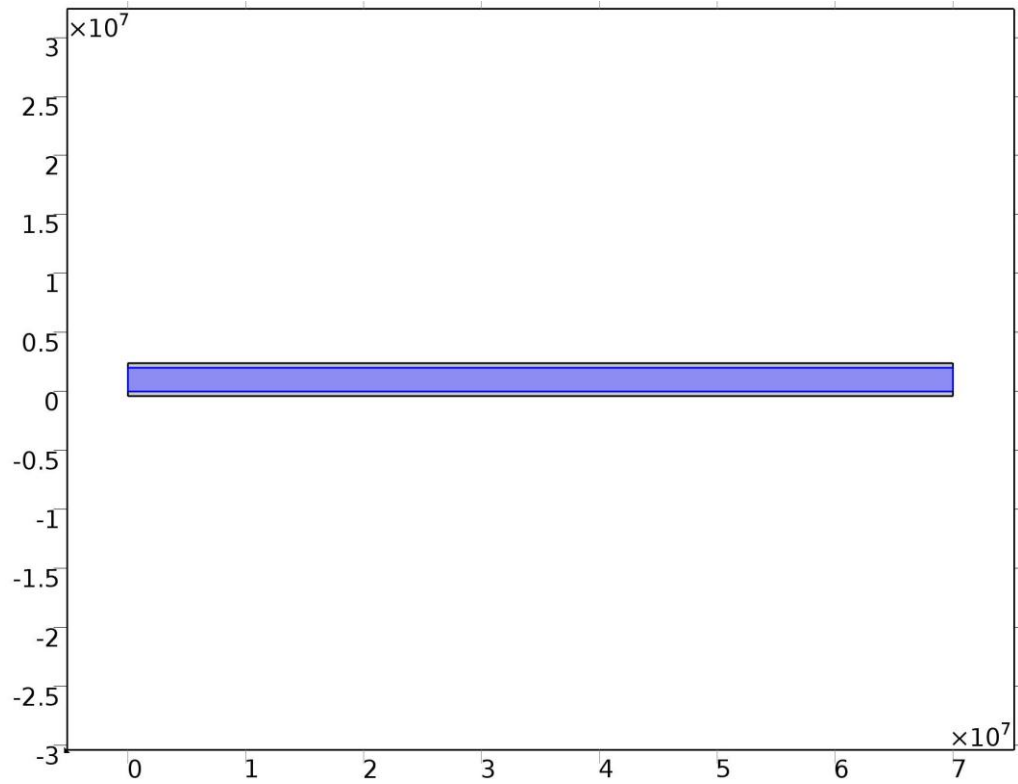


Figure 3.8 Transport of dilute species domain selection (nm).

Table 3.12 Transport domain selection.

Geometric entity level	Domain
Selection	Domain 2

Equations

The initializations of concentration values are based upon the concentration of the cation and the anion species within the polymer domain. The initial concentration and mobility declared in the global parameters effectively determine the final concentration on the domain after the applied electric potential value is obtained from the previous interface and infused into the transport interface. Here C being the ion specific concentration for the concentration of the mobile cation. Mobility is denoted by μ and F the Faraday constant. D_i being the diffusivity of the ion, V is the velocity, Z the charge number and N the Avogadro's number. Here R_i is a corrective term which is particularized for each ion. These equations allow for the tracking of cationic concentration within the model.

$$\nabla \cdot (-D_i \nabla C_i - z_i u_{m,i} F C_i \nabla V) = R_i \quad (6)$$

$$\mathbf{N}_i = -D_i \nabla C_i - z_i u_{m,i} F C_i \nabla V \quad (7)$$

Table 3.13 Transport settings selection.

Description	Value
Concentration	Linear
Value type when using splitting of complex variables	Complex
Frame	Spatial
Compute boundary fluxes	Off
Migration in electric field	1
Convection	0
Convective term	Non - conservative form
Equation residual	Approximate residual
Enable space-dependent physics interfaces	0
Synchronize with COMSOL Multiphysics	

The next module used is the solid mechanics module. Here the necessary conditions are provided to constrain the domains on one side and calculate the displacement on the other tip. The domain selection is given in Table 3.14 and visually in Figure 3.9. The interface settings are given in Table 3.15. The solid mechanics interface computes the body load that is generated by the migration of ions and relates it to the displacement of the domains.

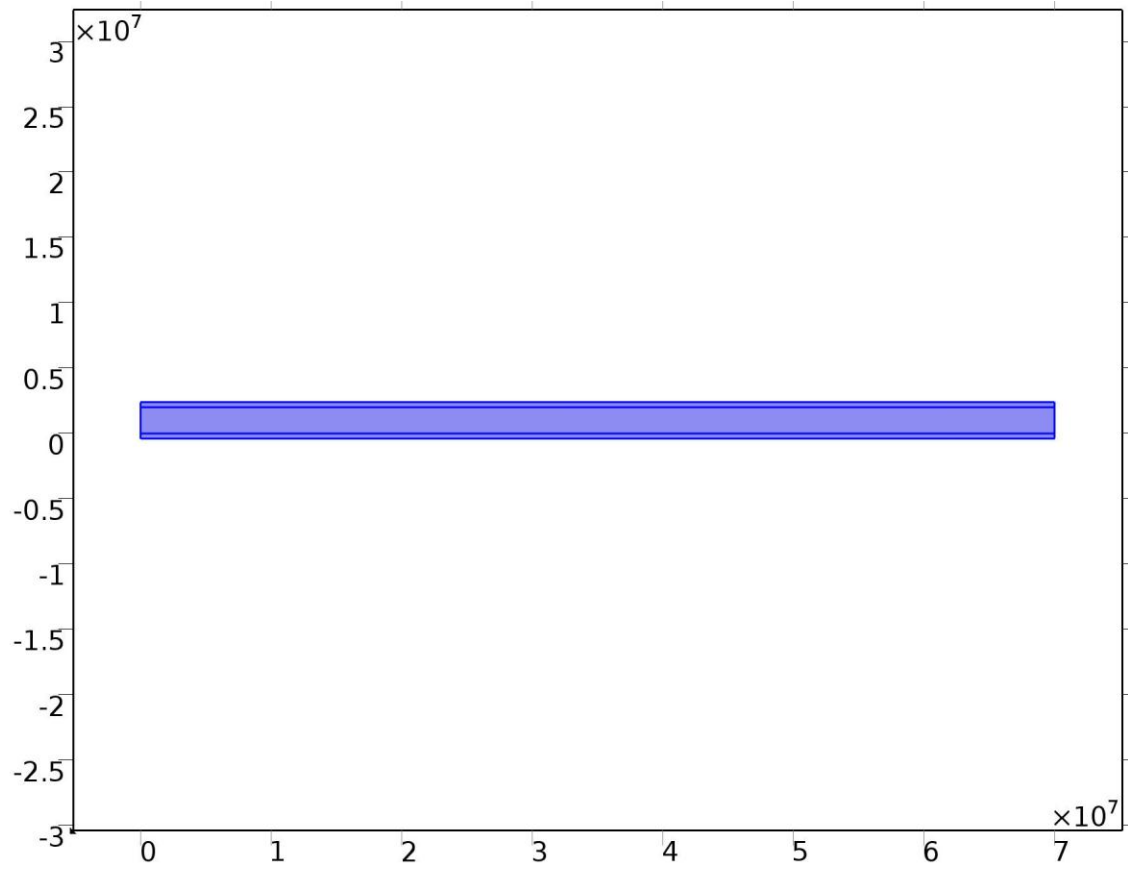


Figure 3.9 Solid mechanics domain selection (nm).

Table 3.14 Solid mechanics domain selection.

Geometric entity level	Domain
Selection	Domains 1–3

Equations

The body load is given by F_v which has been defined previous using the stress value σ that is obtained from the previous models. Here it is to be noted that the body load previously defined is a polynomial fit of the space charge density.

$$-\nabla \cdot \sigma = F_v \quad (8)$$

Table 3.15 Solid mechanics settings selection.

Description	Value
Displacement field	Quadratic
Compute boundary fluxes	Off
Value type when using splitting of complex variables	Complex
Frame	Material
2D approximation	Plane strain
Thickness	1
Structural transient behavior	Include inertial terms
Typical wave speed for perfectly matched layers	solid.cp

The two major constrains for the solid mechanics module are the boundary conditions for the fixed and the free end that is given in the following section. Figure 3.9 gives the free end selections while Figure 3.10 gives the fixed end selections.

3.4.1 Free End

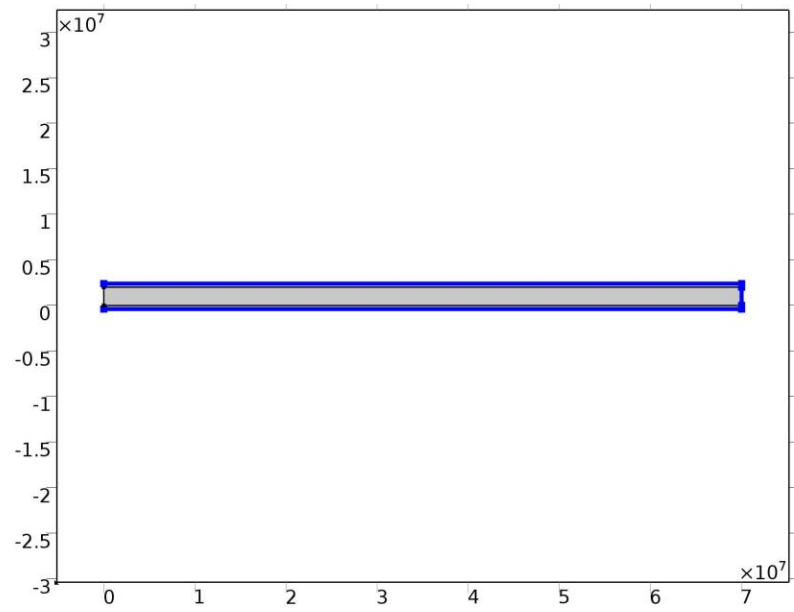


Figure 3.9 Free end constraint selection on the model (nm).

3.4.2 Fixed constraint

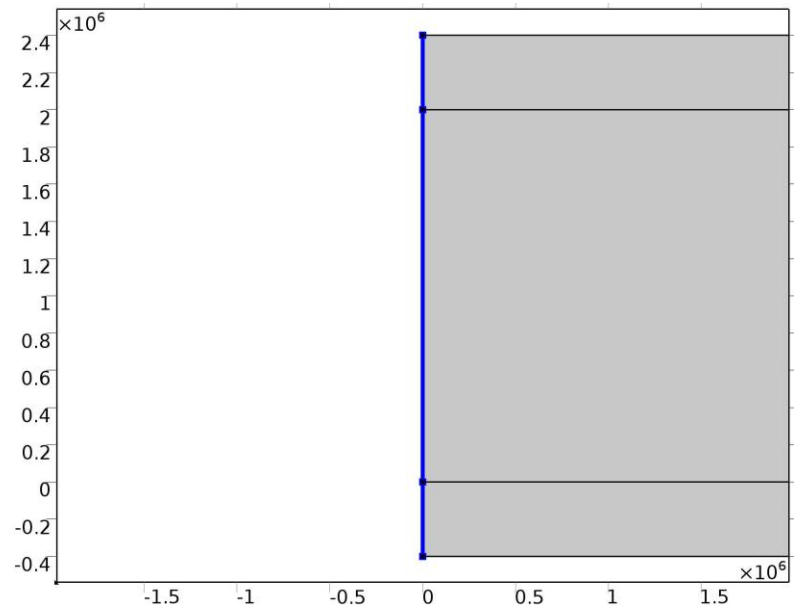


Figure 3.10 Fixed end selection on the model (nm).

3.5 Results

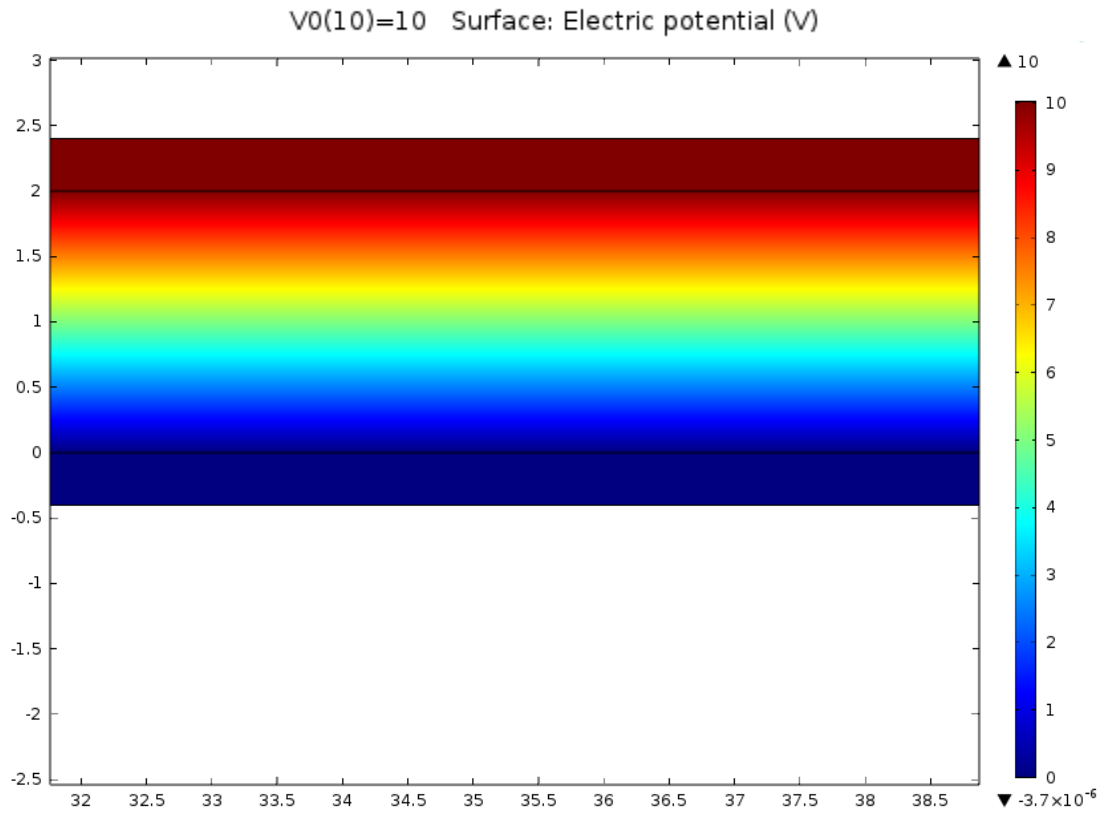


Figure 3.11 Surface electric potential on application of 10V to the model (nm).

The electrostatic results can be seen from Figure 3.11. The sweep function takes the IPMC model from 0 to 10 V using the sweep function. The electric field is spread symmetrically across the section of the IPMC domains.

The electrodes are at 0 and 10 V at the end of the simulation respectively which is captured accurately by the model, while the polymer membrane has a gradient of the electric field across it.

This enables one side to be on the positive potential and the other side to be relatively negative compared to the positive side. It is seen that at the beginning of the simulation the effect is not pronounced and as the simulation progresses, the potential drops at the platinum domains are more pronounced and the electric field shape changes drastically.

As the charged ions migrate across the IPMC, it has been assumed with reasonable understanding that the visualized change was due to the counter current of these migration ions.

This result from the electric current interface is fed into the electrostatics interface to obtain the same results for electric field. Since the values seem to agree with each other and the model is based on feed back coupling, it can be fairly assumed that the models are accurate to acceptable levels.

These values are now fed in to the transport of dilute species model. Here a drastic change in the model variable occurs as seen from Figure 3.12 and hence we need to make sure our concentration distribution works in line with real time experimental results.

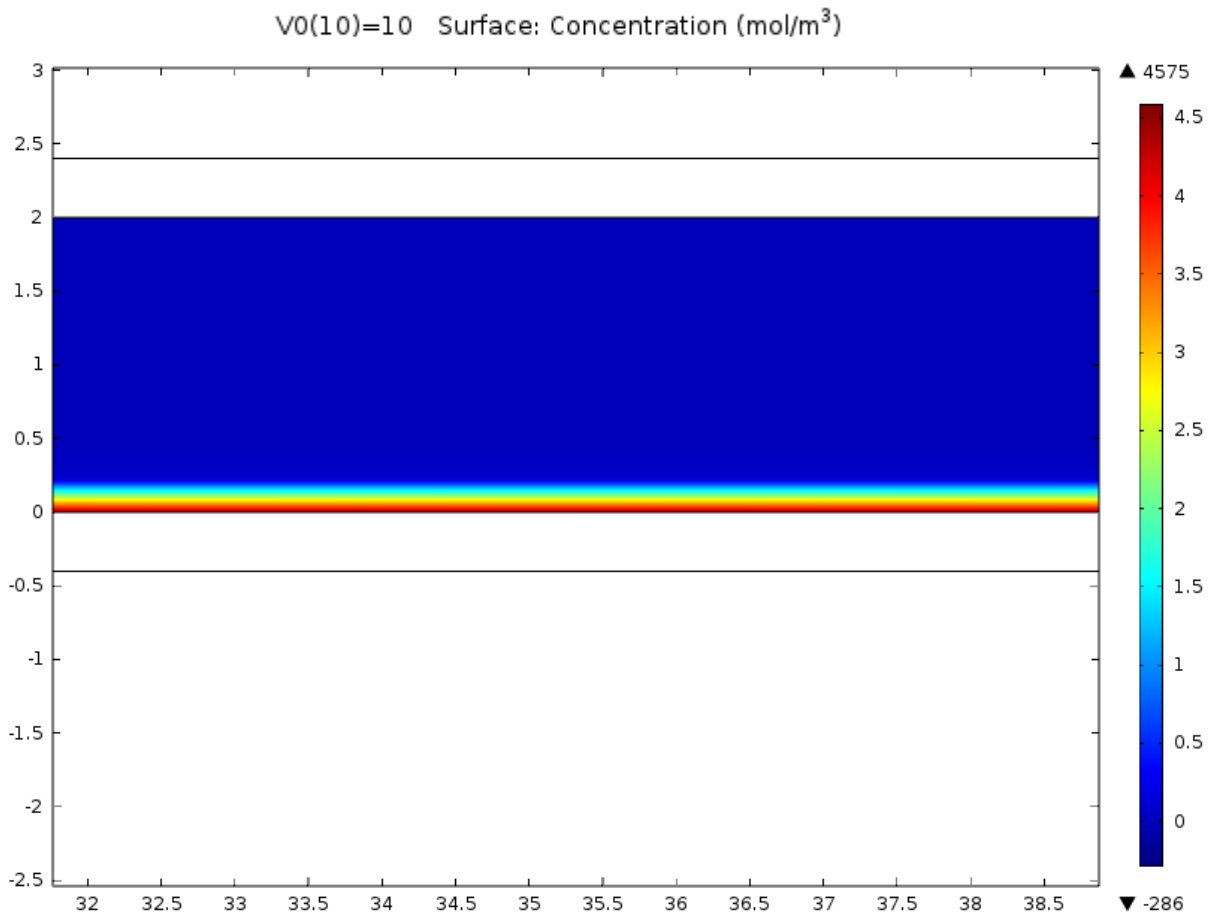


Figure 3.12 Surface concentration gradient on application of 10V to the model (nm).

The transport of dilute species occurs in the Nafion domain alone and the electrodes are isolated from the computation since there is no migration of the charged species within the platinum domain. It has to be noted that the initial concentration of 1200 m/m^3 of cation was placed uniformly across the Nafion domain.

The cations are positively charged and hence will move towards the more negative electrode. Of the two sides, the zero volt side of the electrode is relatively more negative than the positive 10 V. Hence it is seen that the cations are bunching up towards the negative electrode and increase the surface concentration in that region.

The mesh plays a valuable role in this simulation and it can be seen that difference in mesh geometry obtains a difference in the surface concentration of the ions. Hence a refined mesh would give a better result and a more accurate value. This is the reason why a mapped mesh was used to obtain fairly accurate results with acceptable computational time. In actual experimental situations, there exists platinum layer growth within the polymer membrane because of the electroplating process. Since this has not been taken into account and the charged species particle size has not been taken in to consideration, it is extremely difficult to obtain a concentration value over time that would exactly represent the experimental conditions.

Once these results were obtained, it was seen that the solid mechanics interface broke down due to the extremely different young's modulus value of the polymer membrane and the platinum region. There was an accurate capture of the tip displacement values but the visualization of the polymer membrane was not captured accurately. A better model is required to replicate the deformation of the polymer membrane with electrodes on COMSOL. Though the model without electrodes obtained significantly good deformation, the electrode model has to be correlated with other experimental results to obtain individual material properties of the various layers accurately which change due to the manufacturing process.

CHAPTER 4 Experimental Results

Once the COMSOL model was validated, experimental data was collected for the electromechanical analysis of the IPMC. Since the focus was more on getting experimental data, more samples and variations were performed to get the maximum information about the electromechanical properties of various types of IPMCs.

The experimental setup consists of the IPMCs of dimension 70 mm x 8 mm were chosen. These IPMCs had platinum (Pt) electrode with lithium ions (Li^+ ions), Pt electrodes with sodium ions (Na^+ ions) and Bucky paper with imidazolium ions (IM ions).

The IPMCs were clamped on vibration damping stand and holder to minimize the effect of outside vibrations on the actuator's motion.

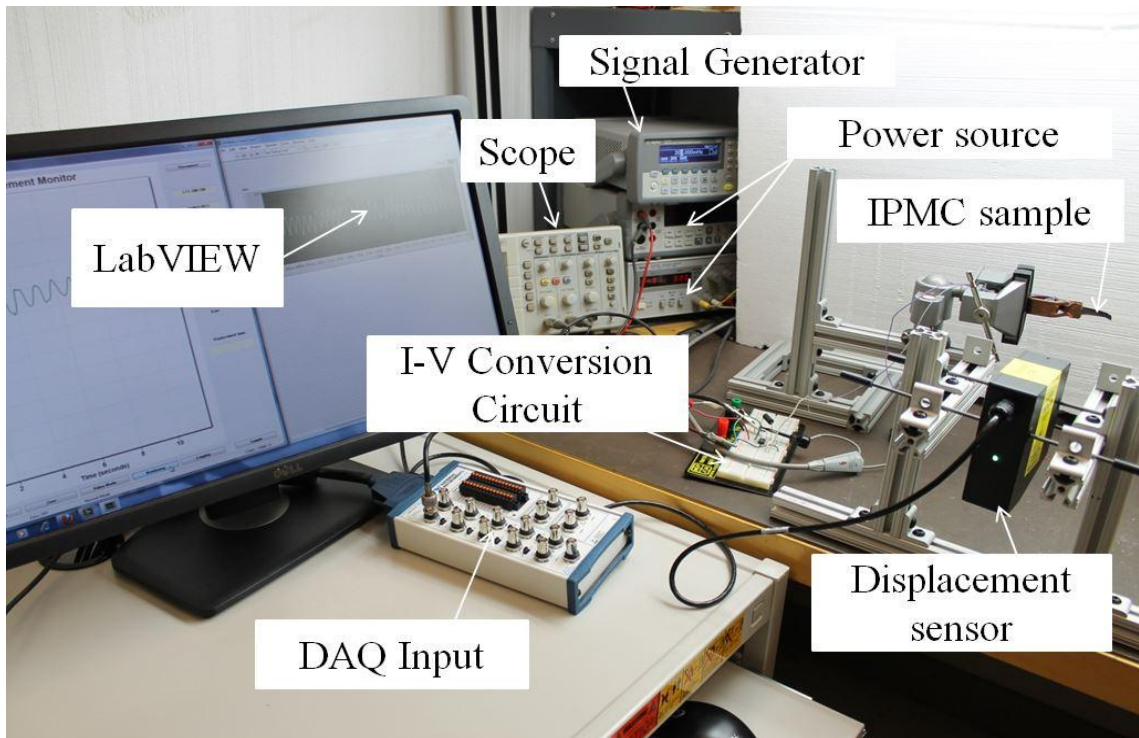


Figure 4.1 Experimental setup showing displacement sensor and current measurement setup.

The tip displacement of the IPMC was measured using a MTI Instruments Inc. (NY, USA), Microtak III, LTS-200-100 displacement sensor which connected to the MT3 support software through an interface as shown in Figure 4.1.

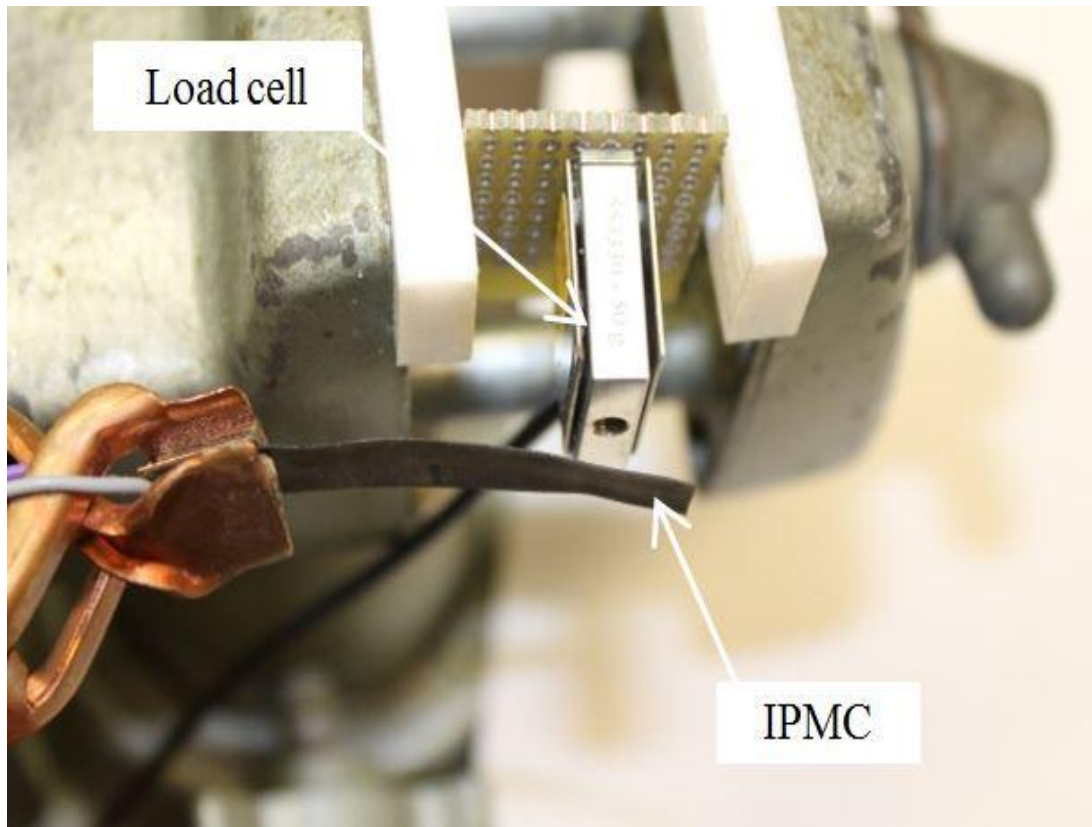


Figure 4.2 Experimental setup showing Load cell – Blocking force measurement setup.

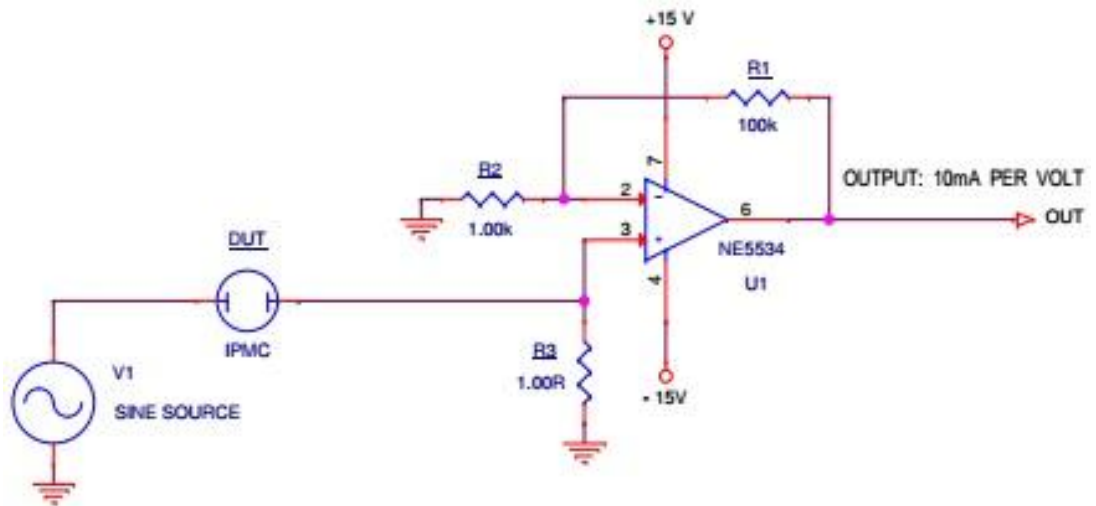


Figure 4.3 Circuit diagram for I to V converter for the measurement of current through the actuator.

A circuit was built to determine the current that was drawn by the actuator for a particular voltage shown in Figure 4.3. This was helpful in determining the amount of current drawn by the platinum and the Bucky-paper IPMC for a particular voltage to obtain the same tip deflection.

The blocking force was measured using a FUTEK (CA, USA), LSB200, 50 g, JR S-Beam Load Cell shown in Figure 4.2. The load cell was attached to an end block to provide the resultant force and the entire setup was clamped onto a vibration damping mount.

The output from the load cell was amplified using a custom built amplifier and the load cell was recalibrated according to the output values of this amplifier. The voltage output values from the amplified load cell signal were multiplied by a factor of 3.19 to obtain the tip force in terms of gram-force equivalent to obtain the blocking force.

This output was taken and fed in to a NI (TX, USA) DAQ with LabVIEW software to monitor the blocking force of the IPMC. The actuation of the system was performed using an Agilent (CA, USA) 33210A. The results were plotted on The MathWorks, Inc. (MA, USA), MATLAB, analyzed and conclusions were deciphered from these plots.

4.1 Displacement Results

Initially the displacement of platinum plated, Bucky paper assembled and gold sputter coated IPMCs were tested. It was seen that the platinum and the Bucky paper IPMCs had significant actuation duration while the gold IPMC underwent extreme electrolysis and the water molecule escaped from the surface of the IPMC actuator.

The rapid electrolysis caused by the application of an electric field on the gold IPMC makes its actuation life very small. This negates any reasonable value to application oriented studies.

Hence a detailed study of the platinum and Bucky paper IPMCs have been done. The calculated displacements from the initial platinum, gold and Bucky paper results are given in Table 4.1.

Since the Bucky paper IPMC contains imidazolium ions and its actuation cannot be included in this table, its values have not been given here. The further studies in detail have been given following it.

Table 4.1 Displacement values for various types of samples tested at 3V constant and averaged over five samples and 5 cycles.

Name	Na⁺ Ion	Li⁺ Ion
Platinum IPMC (Primary coated)	3 mm	3.7 mm
Platinum IPMC (Primary coated)	4.8 mm	6 mm
Gold IPMC Untreated (4 Layers)	0.75 mm	1 mm
Gold IPMC Treated (4 Layers)	1.2 mm	2.3 mm
Gold IPMC Untreated (8 Layers)	1.25 mm	2.35 mm
Gold IPMC Treated (8 Layers)	2.08 mm	3.6 mm

It is to be noted that the gold IPMC actuated for 5 cycles and degraded due to the extreme electrolysis whereas the platinum IPMC and the Bucky paper IPMC were able to sustain their actuation for hundreds of cycles and remain without degradation either in presence of their ionic fluid (as in case of platinum which showed actuation for three days at least in presence of water) and even without the need for hydration as in the case of Bucky paper IPMC.

The actuation was also possible only once and it could not be reused since the sputter coating failed and the electrode layer peeled away from the polymer membrane. This is because of the type of bonding between the electrode and the polymer membrane which is Van der Waals forces. Since these are one of the weakest forces in nature, a clear idea of why the failure occurred seems to reason out. The different failure modes of the IPMCs will be discussed later in this chapter. The more detailed studies were done on platinum and Bucky paper IPMCs.

The IPMCs with both platinum and Bucky paper electrodes were actuated under various voltages and frequencies and their tip deflection and blocking force were calculated and plotted accordingly as seen on Figure 4.4.

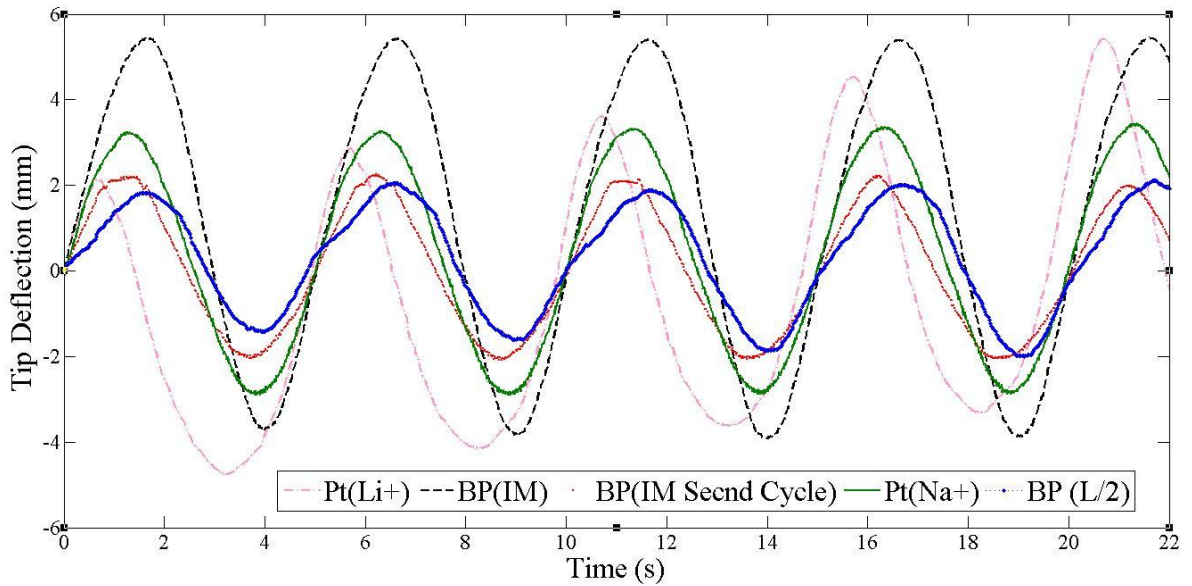


Figure 4.4 Tip displacement measurements as a function of time for Pt (Li⁺ and Na⁺ ions) and BP (IM ions) at 0.2 Hz frequency domain.

IPMCs with platinum electrode and lithium ion (Li⁺) as the cation, platinum electrode and sodium ion (Na⁺) as the cation, Bucky paper electrode and imidazolium ions as cation and Bucky paper with Half length of the original test specimens were tested for their tip displacement at the constant frequency of 0.2 Hz frequency and a peak voltage of 6 V.

It was noted that the IPMC with platinum electrode and lithium ion (Li⁺) as the cation showed a fast tip deflection with the maximum tip displacement of 5 mm. The size of the lithium ions compared to that of the sodium and imidazolium ions might be the reason for the fast actuation since it is smaller and lighter when compared to the other two. This would mean efficient and fast transfer through the cluster chains within the polymer membrane.

The test was again conducted with Pt electrode IPMC with Na^+ as the cation. Though the tip displacement amplitude was of similar magnitude, the response time of the actuator slowed down significantly. This could be explained by the size factor of the molecules once again.

Sodium ions being much larger in size when compared to lithium ions move slower through the sulphonate molecular clusters within the polymer membrane when compared to Li^+ ions. Since the clusters are more densely packed in the course of actuation, it further reduces the velocity of ion transfer from one electrode to another. Bucky paper electrodes on the Nafion membrane were tried in two different configurations.

In the first trial the IPMC with BP electrode and imidazolium (IM) ions seemed to give a vast increase in the magnitude of the tip displacement. Though the actuator provided a large bending deformation, the response time was again slow owing to the size of the imidazolium ions.

A second cycle of the BP IPMC was run to obtain the reduction in the amplitude of the tip displacement. One cycle of actuation was taken as 250 oscillations of the membrane for measurement purposes. The actuation was seen to significantly reduce in amplitude as well as slow down as a function of time but in a nonlinear fashion.

Though the main motive of using the Imidazolium ions is to reduce the effect of electrolysis the surface which would evaporate the water molecules involved in requiring the IPMC to be rehydrated, they seem to be affected by membrane fatigue or electrolysis themselves which prevent further actuation of the IPMC. Another test was run with a

shorter BP electrode IPMC. The original length of 70mm was reduced to 30mm in order to obtain a smaller and a stiffer IPMC.

The main motive of this study was to obtain the maximum blocking force using the stiffer IPMC. A very large blocking force of 2.52 gF was obtained but the tip deflection amplitude and the response time were traded off in this particular study which was adverse for application purposes.

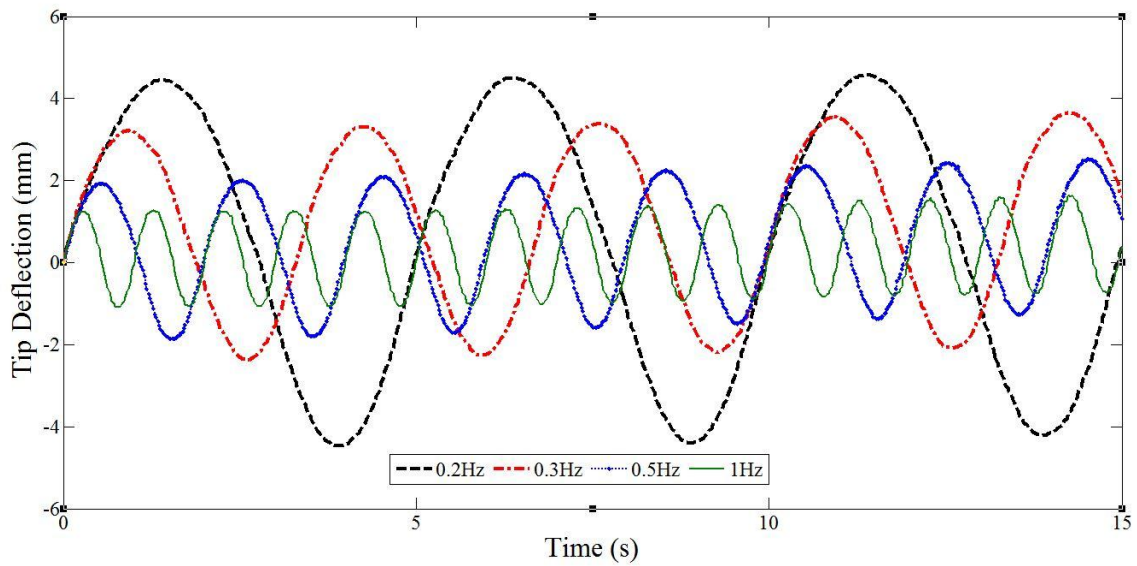


Figure 4.4 Tip displacement measurements as a function of time for BP electrode IPMC with IM ions for varying frequency domains.

Having obtained the largest amplitude from a fixed frequency study, the BP electrode IPMC was tested for varying frequency domains from 0.2 Hz up to 0.5 Hz.

From Figure 4.4, it was observed that the frequency domain change introduced a large change in the amplitude of the IPMC's tip deflection. As the frequency increased, the amplitude was noted to reduce significantly with each varying change of 0.1 Hz.

There was significant reduction in the tip displacement amplitude with increase of frequency but the bending deformation response to that of the input signal was observed

to be very constant. Though the voltage was maintained the same, BP electrode IPMC actuator seemed to perform better than the other samples that were tested. The reason for this would be that their actuation was fairly linear.

The varying frequency domain tests were performed on a platinum electrode, containing Li^+ ions as the cation, to see the variation in the amplitude of the tip deflection in the actuator. It was noticed from Figure 4.5 and Figure 4.6 that the IPMC was showed significant relaxation behavior after the actuation.

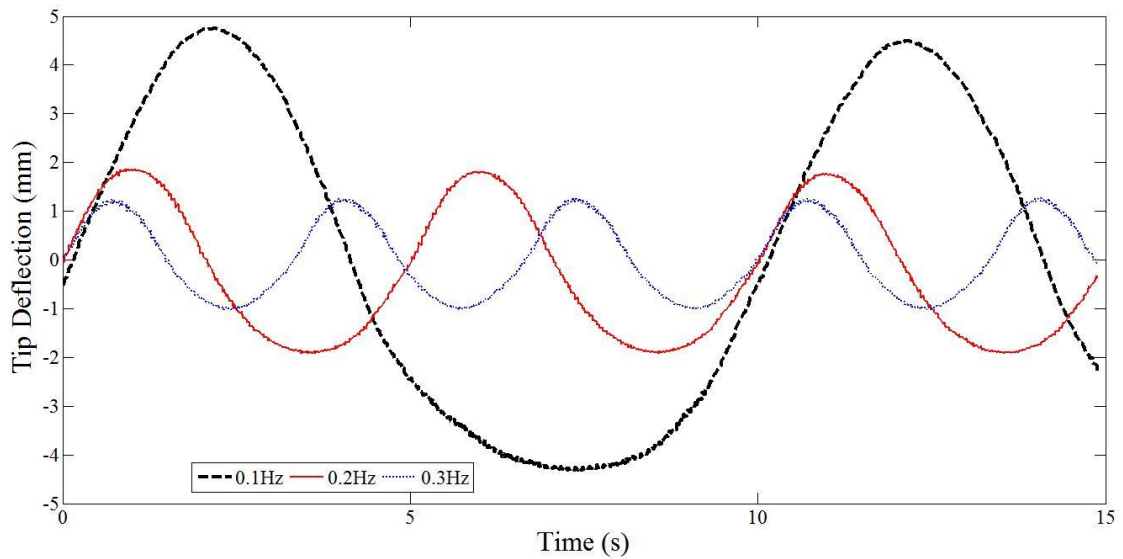


Figure 4.5 Tip displacement measurements as a function of time for Pt (Li^+) for varying frequency domains.

Though the actuation was fairly large with respect to the tip deflection magnitude, the polymer actuator tended to actuate more towards one side and had a very common pattern of actuation and relaxation rather than actuating in both directions.

In general it was noted that the amplitude of the tip deflection decreased with time. This is caused by electrolysis occurring due to the electric field through the

membrane which is adverse to IPMC actuation. It dries out the polymer and the membrane needs to be hydrated and swelled again.

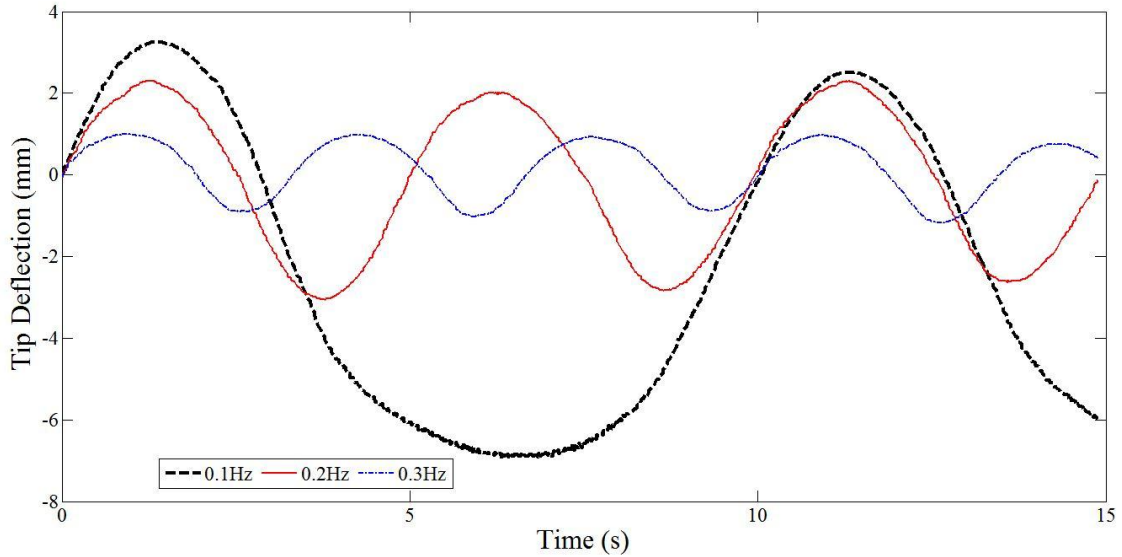


Figure 4.6 Tip displacement measurements as a function of time for Pt (Na⁺) for varying frequency domains.

The sodium ions (Na⁺) were then tested for their performance in varying frequency domains.

Though they exhibited similar deflection patterns, following closely the trend of the deflection attained with lithium ions, it was noted that the relaxation was significantly lower than that of the lithium ions.

This might be due to the accumulation of the heavier charge particles and saturation on the electrodes which reduces the relaxation factor per se but actuation occurs due to the dispersed ion clusters within the membrane.

The tip deflection though uniform for a particular time period, depends extensively on multiple variable factors and hence acts very non-linear in terms of both the strain (due to ion transfer and deflection) and blocking force.

4.2 Blocking Force and Current Consumption Results

The blocking force determines the amount of force that an IPMC can effectively produce in a constrained environment to act on an external system. A load cell arrangement as displayed in Figure 4.2 is used in the measurement of this blocking force.

The blocking force measurements were taken in series with the tip deflection caused by varying the voltage domain on different IPMC samples.

The blocking force values were averaged over 5 readings to account for the non-linearity of the IPMCs and to resolve any percentage of error in measurements to a negligible margin.

The current required was measured using a current sense resistor connected in series with the IPMC. The value of this sense resistor was chosen small enough to ensure that it does not affect the current through the circuit shown in Figure 4.3. The designed gain of the circuit was around 0.11 A/V.

The current consumed was measured using a scope as well as a signal digital multi-meter to ensure credibility of the measurement. The current drawn by different samples of IPMCs under given varying voltage domain from 1 V_{p-p} to 10 V_{p-p} was plotted as a graph.

The samples were measured for the blocking force and the current consumption simultaneously using integrated systems and a LabVIEW code.

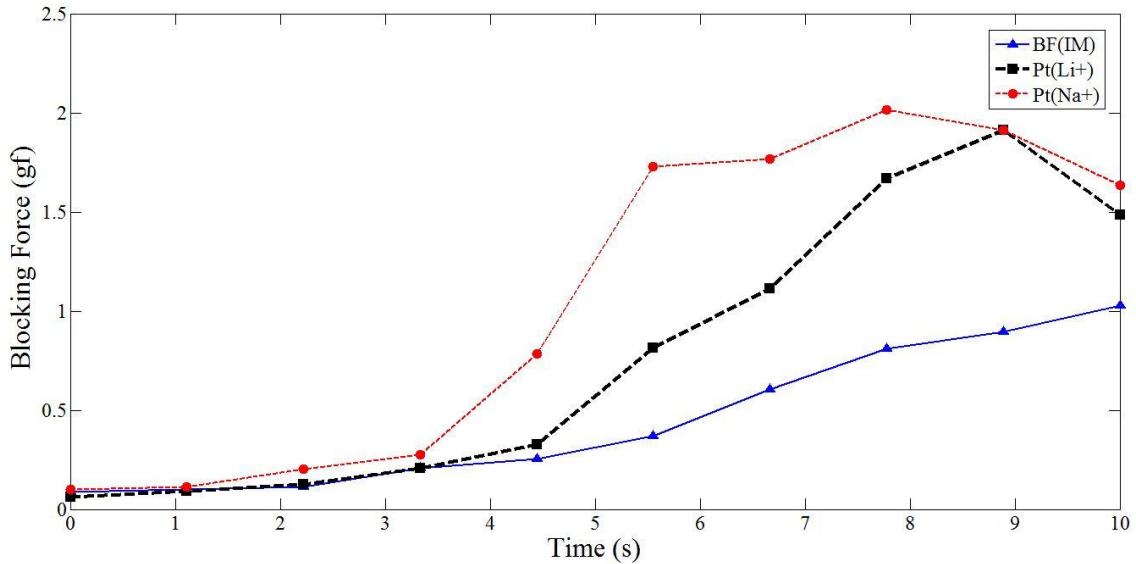


Figure 4.7 Blocking force measurements as a function of time for various IPMC samples.

The blocking force was measured for the three different samples of IPMC as before – BP (IM), Pt (Na⁺) and Pt (Li⁺) combinations respectively.

The Pt electrode with sodium ions gave the largest blocking forces in terms of gram-force as seen from Figure 4.7, since their ion size was optimized for both optimal deflection and optimal tip force.

Though the Pt electrode IPMC with lithium ions showed similar trend, the values of the tip force was slightly lower compared to that of the sodium ions. But in both the cases, after a particular threshold voltage, the blocking force reduced drastically because of excessive charge accumulation on one side of the polymer membrane which causes relaxation of the membrane leading to charge saturation.

On the other hand, the BP IPMC with imidazolium ions showed significantly smaller blocking force without relaxation on a slightly higher voltage range comparatively. Though the blocking force was much lower than the Pt ion IPMC, the tip displacement was found to be much higher than the Pt electrode IPMC with sodium and lithium ions.

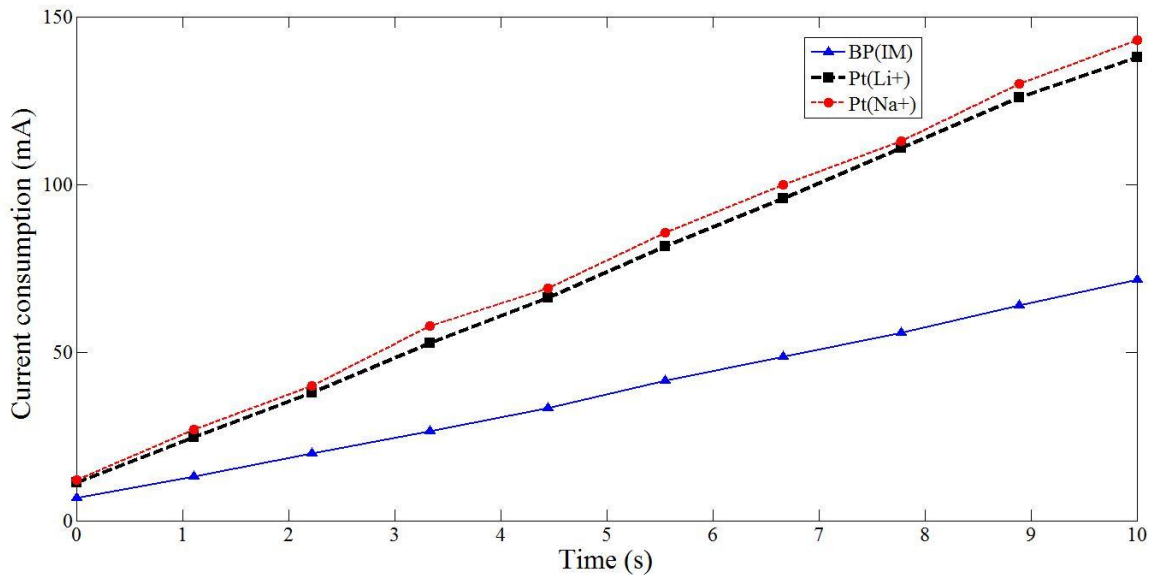


Figure 4.8 Current consumption measurements as a function of time for various IPMC samples.

On the other hand, when comparing the voltage input to the current consumed by the IPMCs for a varying voltage domain, it is seen that the BP (IM) IPMC consumes the least current (i.e. requires the smallest power for actuation even at higher voltages compared to the Pt electrodes with either sodium or lithium ions).

As seen from Figure 4.8, The current consumption for the Pt electrode IPMCs show a very significantly close trend giving the impression that the electrode material plays a more important role in the current consumed when compared to the ion content or ion size that exists in the electrolyte. This can be further extended to imply that the

transported charge and the charge accumulation on the electrode is independent of the ionic liquid and depends more on the electrode material and morphology in this particular study. This serves to be an important factor since an optimized electrolytic system of mixed ionic content can be further looked into while maintaining a constant yet efficient electrode based on the electrode morphology.

4.3 Electrode morphology and failure study

The electrode morphology studies and the failure analysis of the electrodes are done using Scanning Electron Microscopy (SEM) and Energy Dispersive X-ray Spectroscopy (EDS). The SEM is performed using a FEI (OR, USA), Quanta 650 Scanning Electron Microscope that is fitted with a Bruker (MA, USA), EDS detector. The electrodes show varied coating shapes based on the type of deposition / coating used. This would be helpful to understand better how the electromechanical properties are affected due to the electrode morphology.

4.3.1 Gold electrode morphology

The gold sputter coating is analyzed first using SEM and EDS. It is seen from Figure 4.9 to Figure 4.12, the four and eight layers of gold sputter coated IPMCs are analyzed at two conditions namely treated (wherein the Nafion membrane has been sandblasted and ultrasonically washed before sputter coating) and untreated (untouched Nafion membrane).

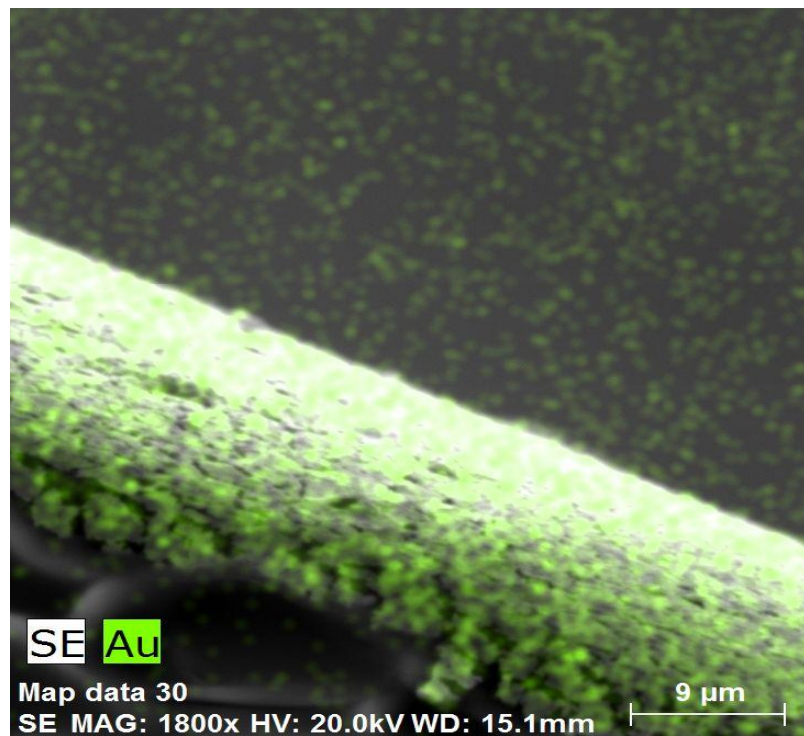
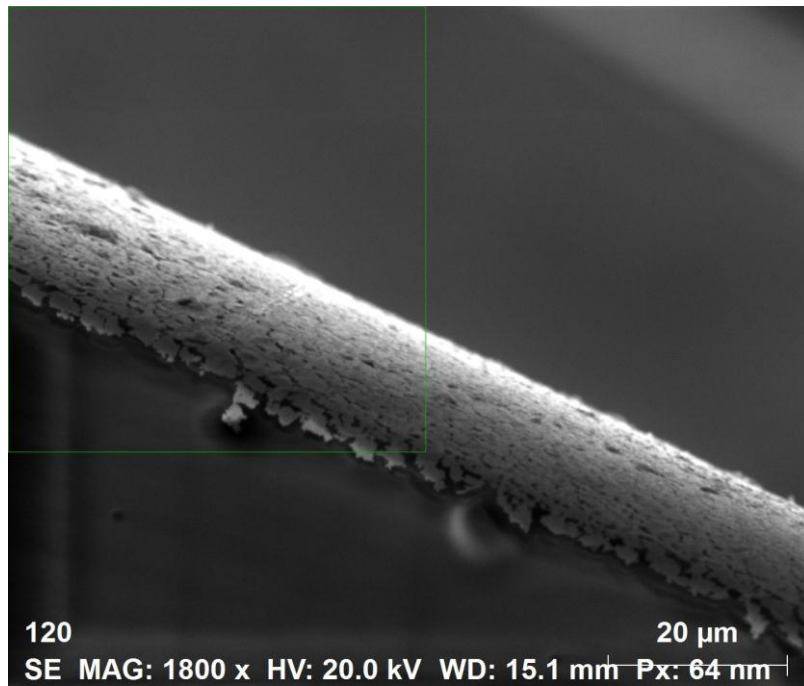


Figure 4.9 (Top) SEM image and (Bottom) EDS image of un-treated 4 layer gold sputter coated sample. Green color denotes gold.

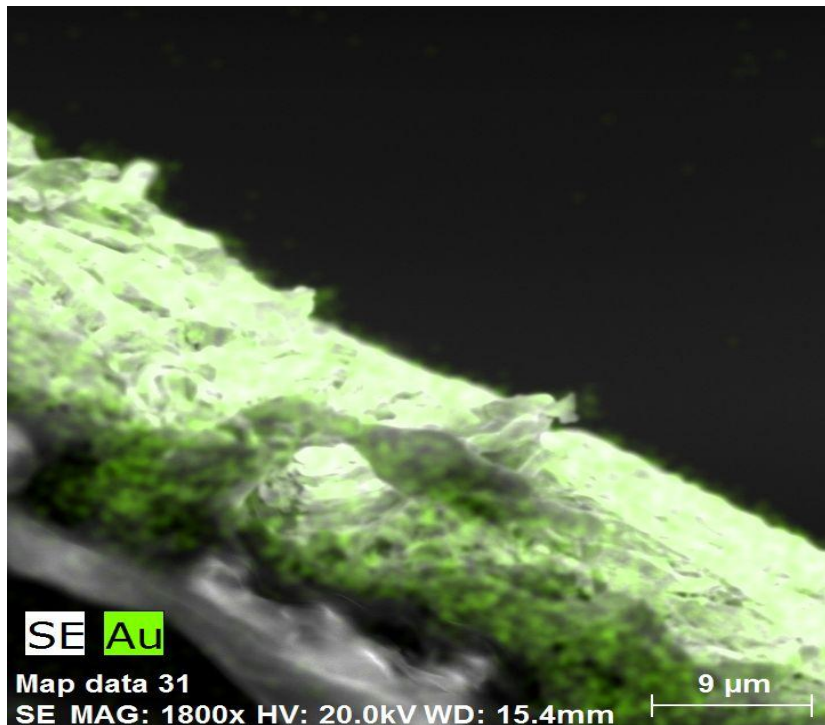
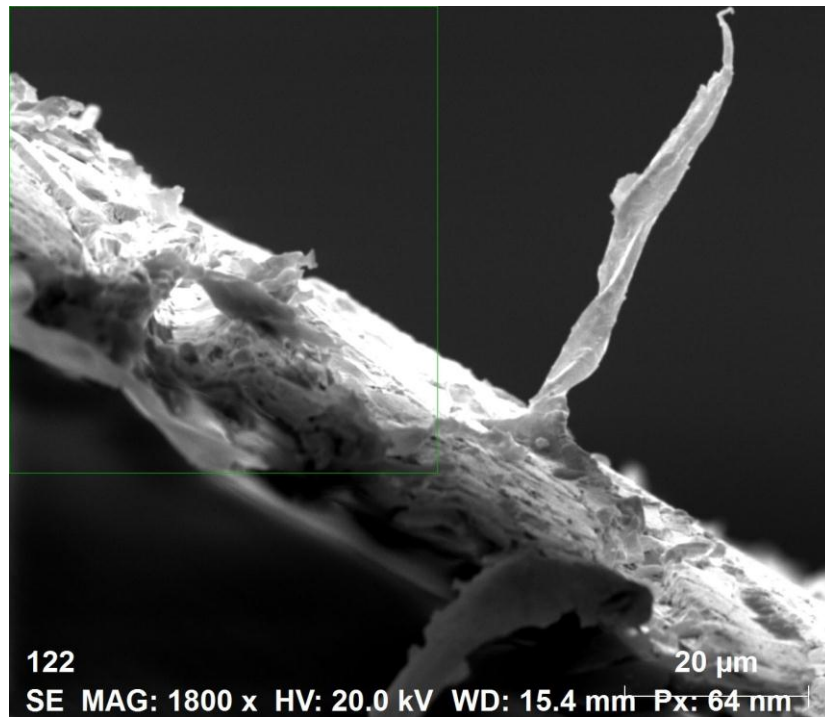


Figure 4.10 (Top) SEM image and (Bottom) EDS image of treated 4 layer gold sputter coated sample. Green color denotes gold.

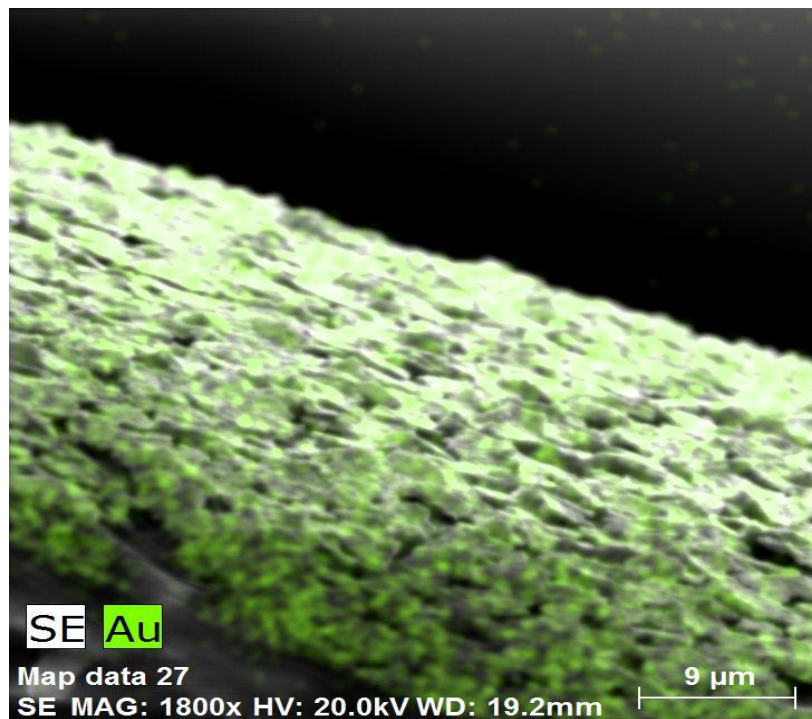
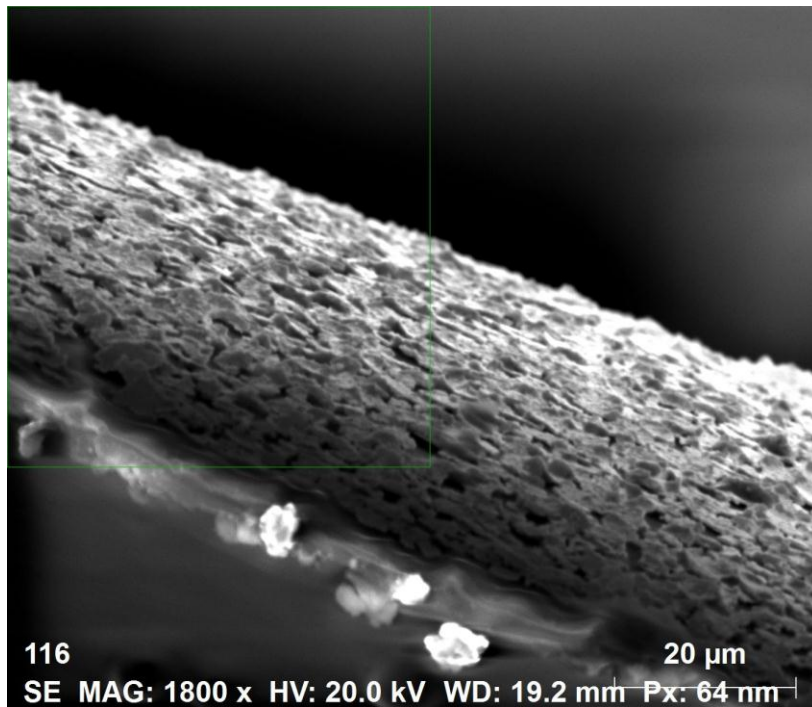


Figure 4.11 (Top) SEM image and (Bottom) EDS image of un-treated 8 layer gold sputter coated sample. Green color denotes gold.

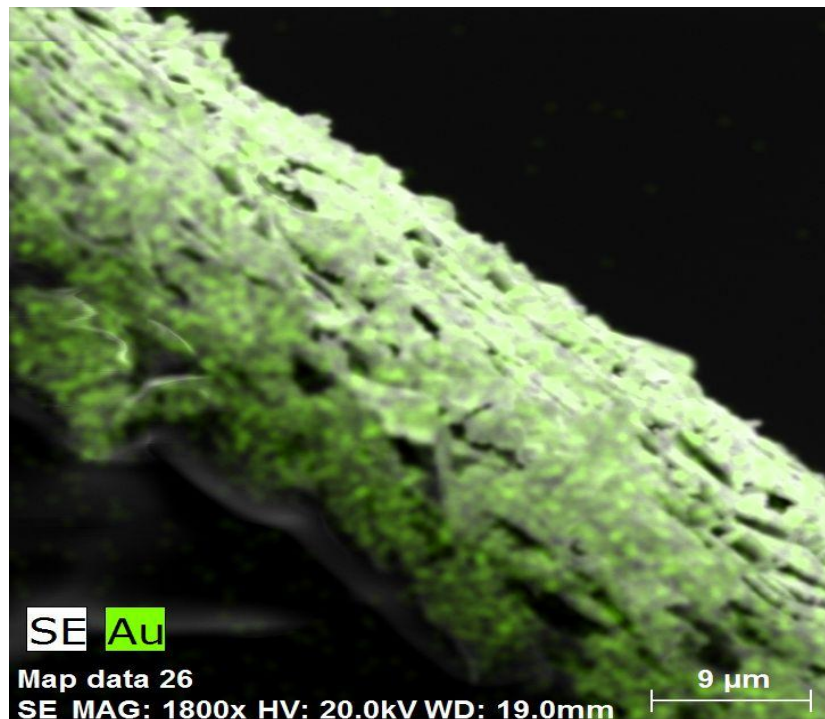
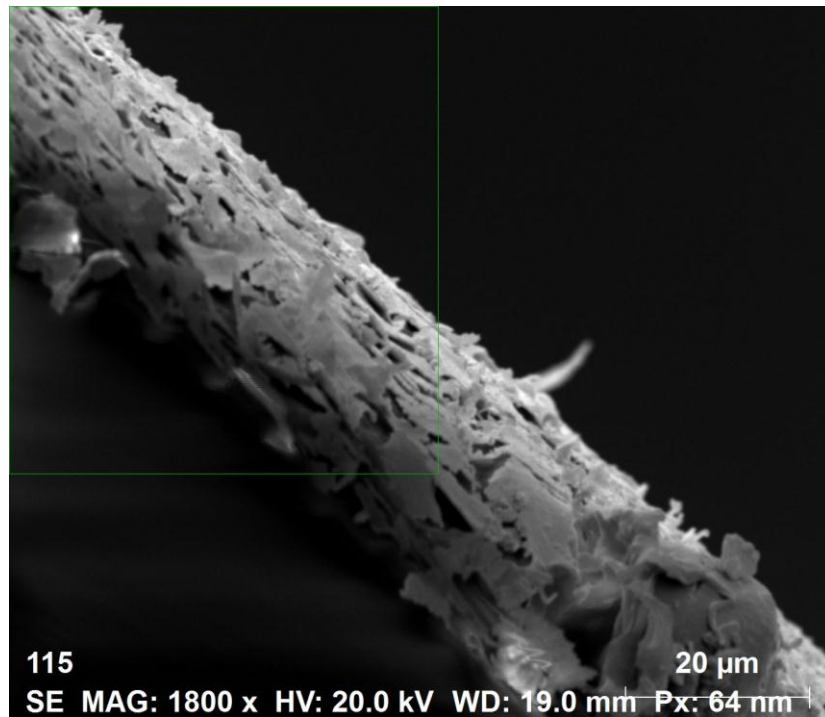


Figure 4.12 (Top) SEM image and (Bottom) EDS image of treated 8 layer gold sputter coated sample. Green color denotes gold.

It can be seen from the above images in Figure 4.9 to Figure 4.12 of the gold sputter coated samples, that the treated surfaces are much rougher compared to the untreated samples. This may be due to the striations found on the surface of the polymer membrane when it was sanded and ultrasonically washed. These striations cause surface roughening, which in turn increases the friction coefficient of the membrane. Thus the higher energy surface holds the gold sputter coat better than the smooth surface of the membrane.

This surface roughening causes an uneven distribution of the gold sputter coat as compared to the smooth surface (i.e. the untreated surface). This uneven distribution leads to a principle of flake piling, an effect of gold flakes or gold sputter coat particles clouding onto the surface in an uneven manner that increases the electric charge density on the surface.

This causes a significant change in the electric field distribution on the surface and causes better deformation as compared to the smooth surface. The results of this can be seen from the Table 4.1 in the beginning of the chapter.

4.3.2 Bucky paper electrode morphology

The Bucky paper electrode is electrode plated through the direct assembly process shows much better bonding compared to the gold sputter coated sample. This is because of the method of assembly that has been used and the difference in the forces that holds the electrodes to the polymer membrane.

The Bucky paper IPMC was analyzed under both SEM and EDS detectors and the images were obtained to study the electrode shape and morphology which is further elaborated using 3-D surface plots using a Hirox digital microscope to study its failure modes.

Though there seems to be significant gaps in the contact surfaces as seen from Figure 4.13 between the Bucky paper and the polymer membrane, it has to be noted that the carbon nanotubes seem to adhere to the polymer membrane like hooks onto a cloth, which enables extremely tiny strands that are detected within the polymer membrane cross section to hold the Bucky paper really rigid on to the surface of the polymer membrane.

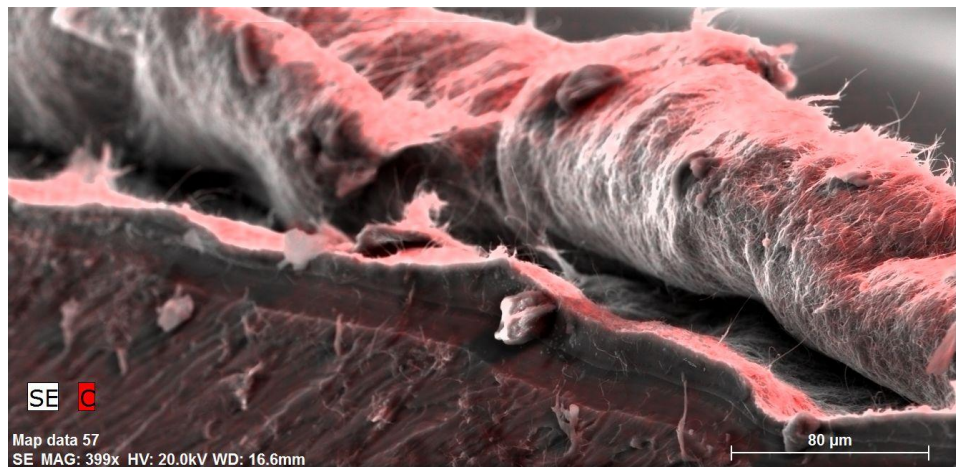
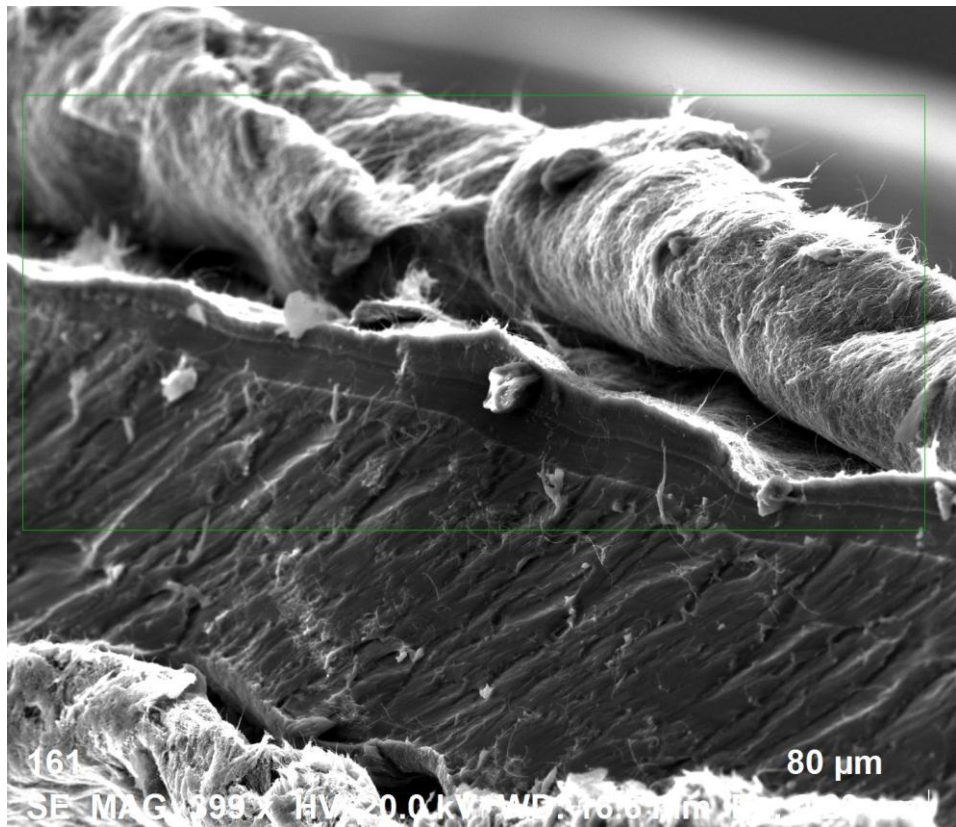


Figure 4.13 (Top) SEM image and (Bottom) EDS image of Bucky paper IPMC sample. Red color denotes carbon.

4.3.3 Platinum electrode morphology

The platinum IPMC samples were next tested on the SEM and EDS systems. There were two samples of the platinum. One was the primary coated IPMC sample which was not developed and the second sample was the developed or the secondary plated IPMC sample.

These platinum coats as seen on Figure 4.14 and Figure 4.15 can be compared to the 4 layer and the 8 layer gold sputter coating on their thickness ratios. The primary sample in essence plates only an extremely small layer of platinum on the surface of the polymer membrane wherein the secondary plating or the development process causes the growth of platinum layer to a larger extent. It can be seen from the SEM and EDS images that the primary coat looks extremely soft with regards to the texture of the coating. It is smaller as well as much milder in surface features when compared to the secondary coating. On the other hand, the secondary coated or the developed IPMC sample displays a stronger and a more matured growth of the platinum layer on the surface. The texture is well defined and looks to be much harder compared to the primary coat. Though in essence this should increase the stiffness of the IPMC actuator, it is seen that this causes a positive response of increasing the displacement because of increased charge density and also increases the blocking force of the IPMC sample.

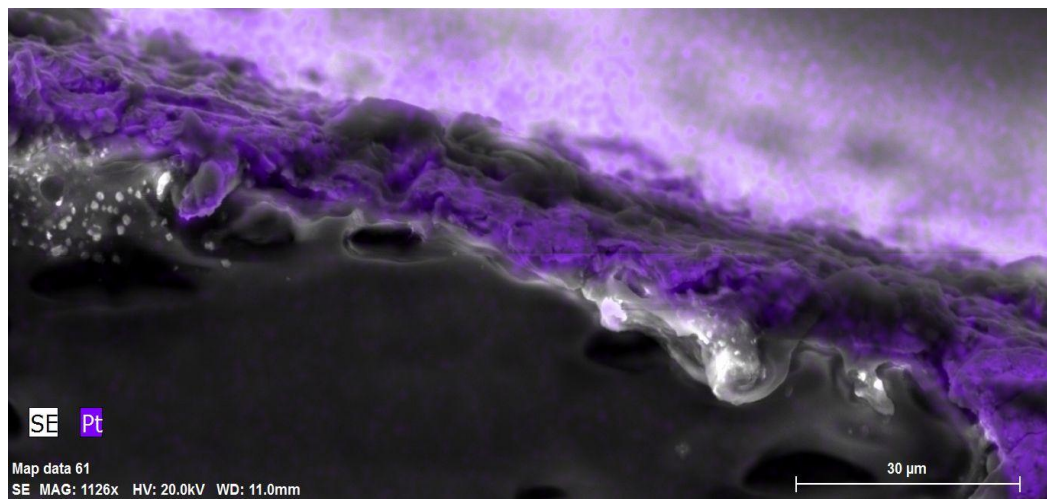
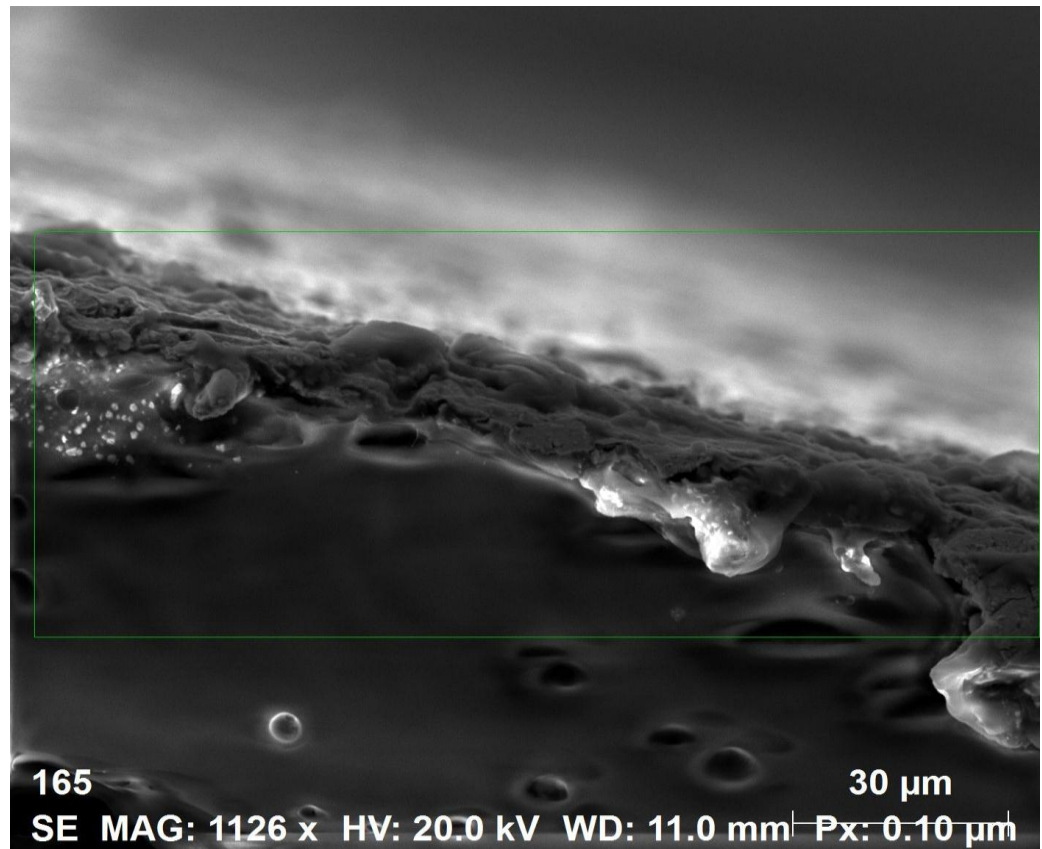


Figure 4.14 (Top) SEM image and (Bottom) EDS image of platinum primary coated IPMC sample. Purple color denotes platinum.

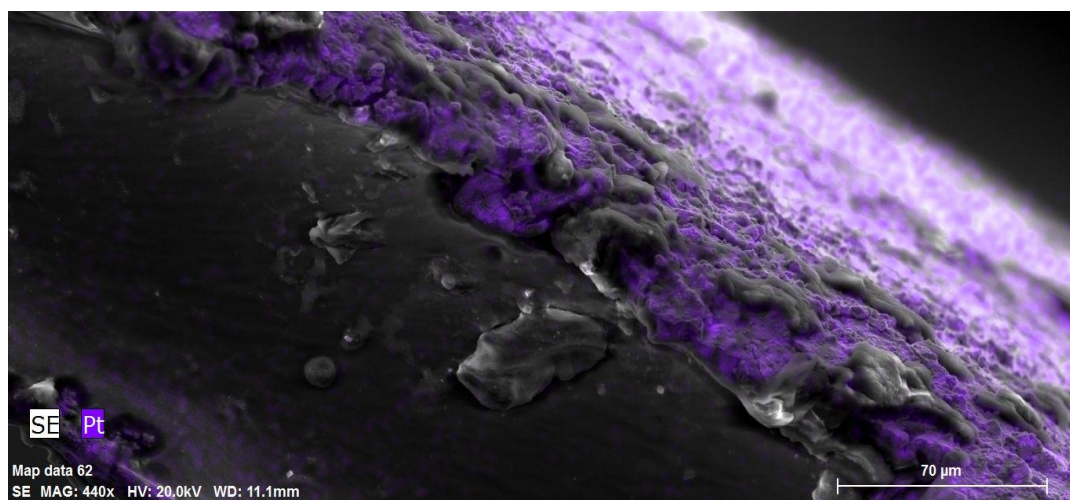
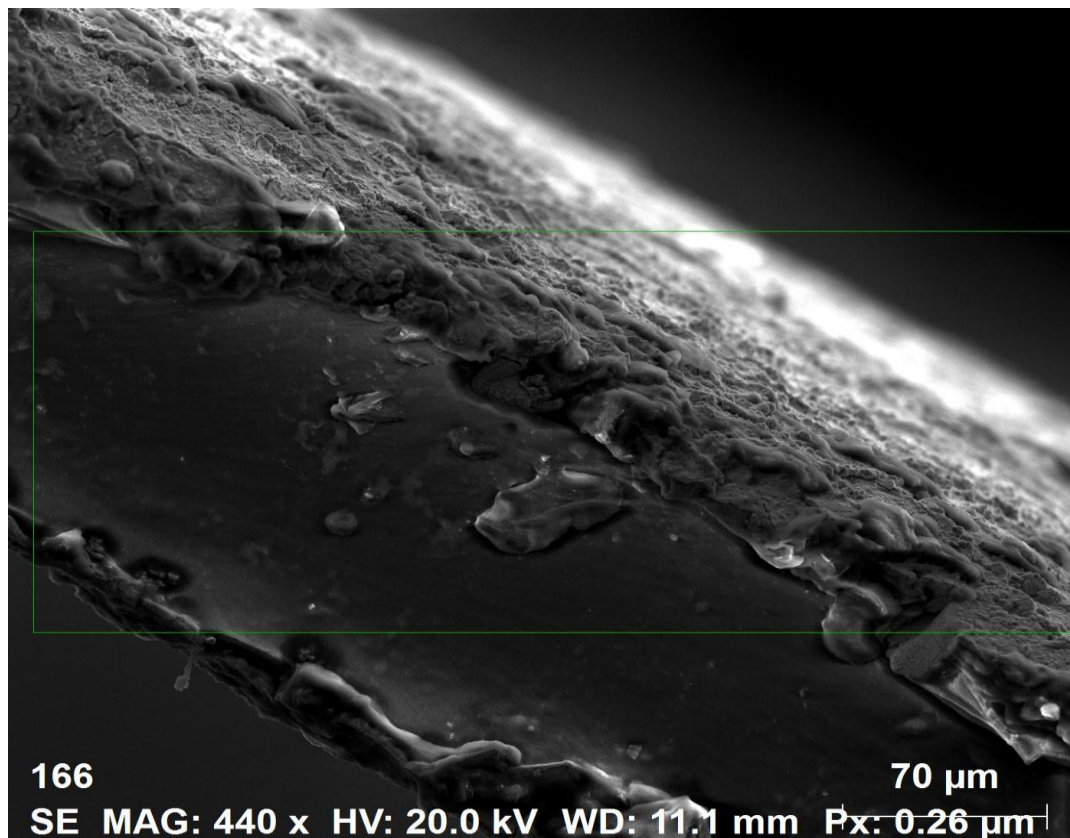


Figure 4.15 Figure 4.14 (Top) SEM image and (Bottom) EDS image of platinum secondary coated IPMC sample. Purple color denotes platinum.

4.3.3 Gold electrode failure

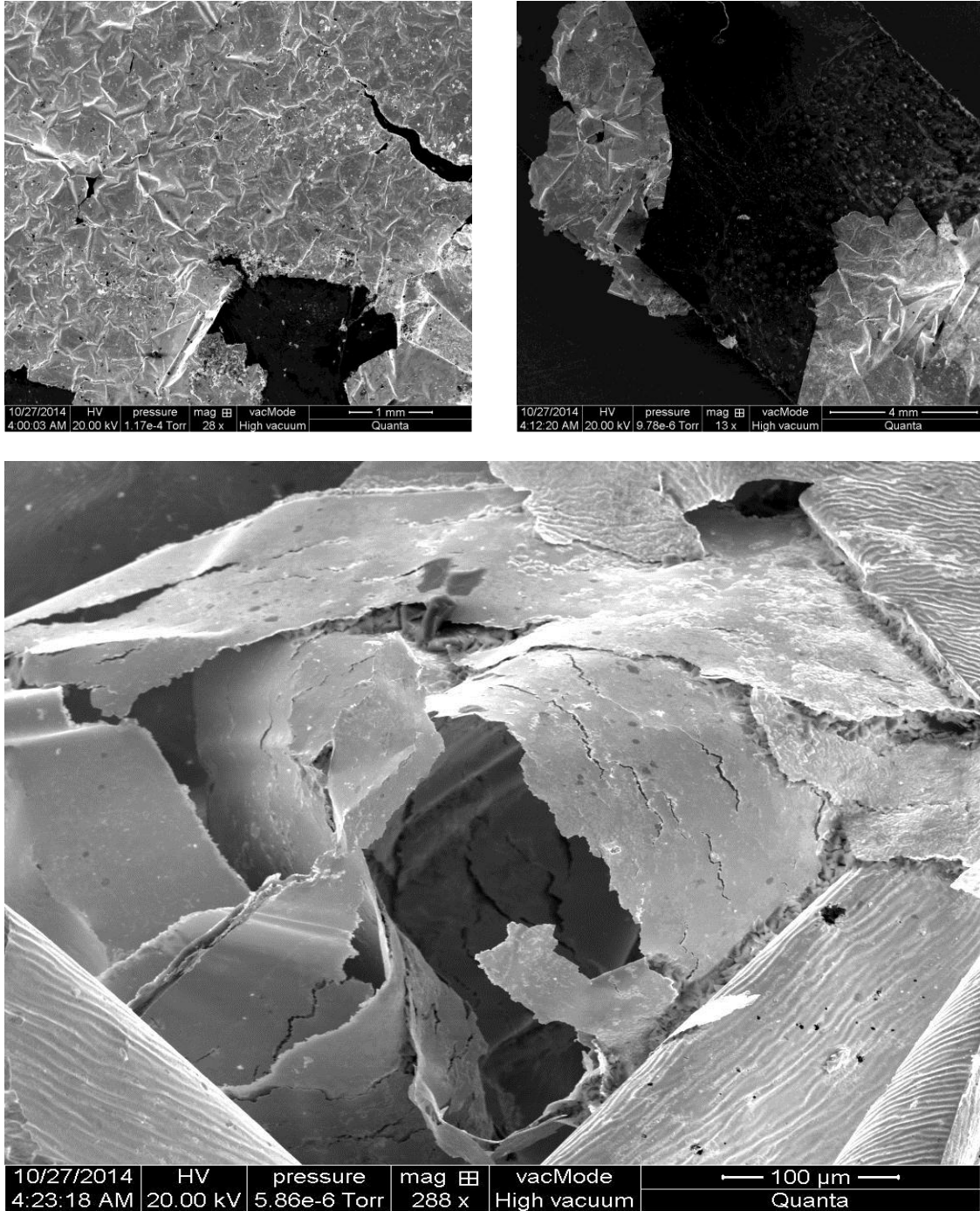


Figure 4.16 Various zoom levels of the gold sputter coated electrode breaking and peeling off after five actuation cycles.

The gold sputter coated sample was extremely feeble when it came to bonding as well as actuation. Not being very effective it was seen that the sample peeled off as seen from Figure 4.16 and did not show out to be as robust as the other electrodes.

Though it has already been discussed preciously why this failure mode occurs, reasoned to the fact that the forces holding it together are weak, this SEM imaging helped throw another perspective to the whole gold electrode issue. It is seen that apart from breaking off the surface of the polymer membrane the gold electrodes, being deposited as flakes, start breaking within themselves. Since they aren't deposited as a single entity and are just sputtered down from a target, there is nothing to hold them in place as a single electrode the way Bucky paper holds.

This gives another ideation of how this failure mode could be tackled. If there is an external adhesive unit that can be mixed with the inert gas mixture that would be electrically repulsive to the target cathode, this would push the adhesive particles on to the membrane and allow for the bonding of the sputter particles themselves as they get deposited on the surface.

This being complex, a simpler solution would be to coat the sample layer with an adhesive coating before sputter coating to enable better bonding between the particles and the polymer membrane.

4.3.4 Bucky paper Electrode Failure and comparison with Platinum

Pt electrode and BP electrode IPMCs were studied for their electrode morphology under a Hirox (Tokyo, Japan), KH-8700 Digital Microscope and the surface and cross sectional images were 3-dimensionally plotted and measured. These electrode morphology studies, apart from showing various issues such as delamination and debonding occurring in the direct assemble process, also gives the plating efficiency and the thickness of each electrode and their uniformity both along the surface as well as through the cross section.



Figure 4.17 Surface image of overlapping layers due to delamination in Bucky paper IPMC.

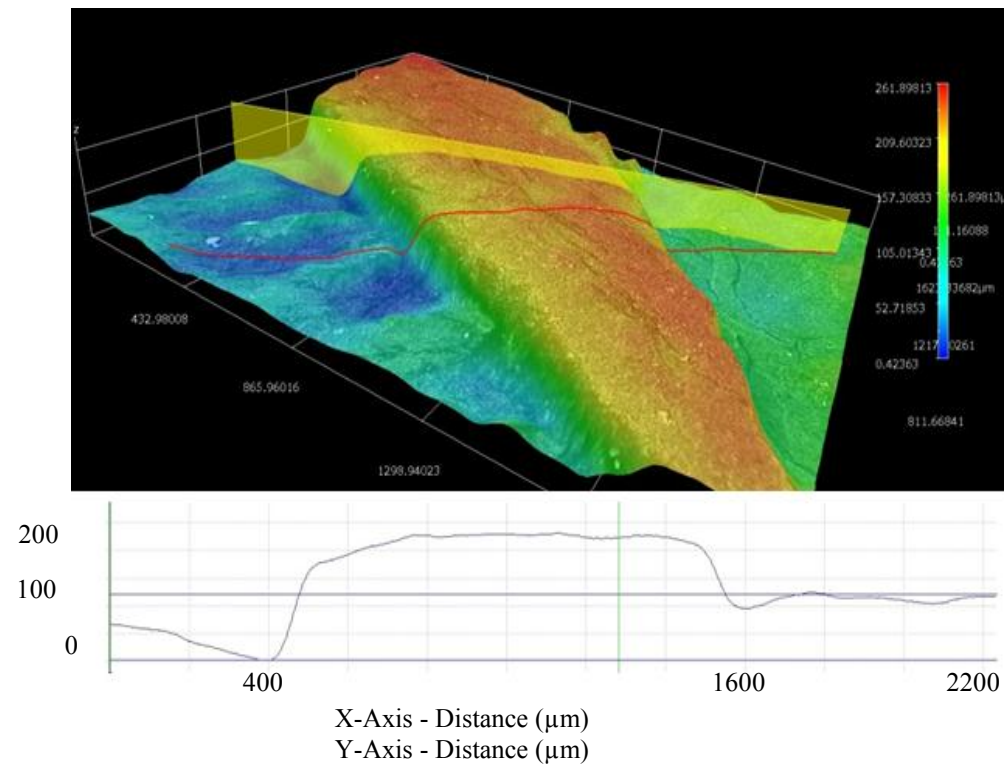


Figure 4.18 Pseudo color image and 3-D surface plot with local maxima and minima of the failure.

In BP-IPMC, it was most commonly found that the Bucky paper electrodes were subjected to delamination with use and handling. This was because of the nature of the soft bonding between the perfluorinated membrane and the Bucky paper electrodes. Figure 4.17 and Figure 4.18, show the partial delamination of the Bucky paper electrode from a sample perfluorinated polymer membrane bonded with Bucky paper.

Apart from this it was also found from Figure 4.19 and Figure 4.20, that the electrode surface area was more uniform in case of chemically coated Pt electrode in comparison with Bucky paper electrodes.

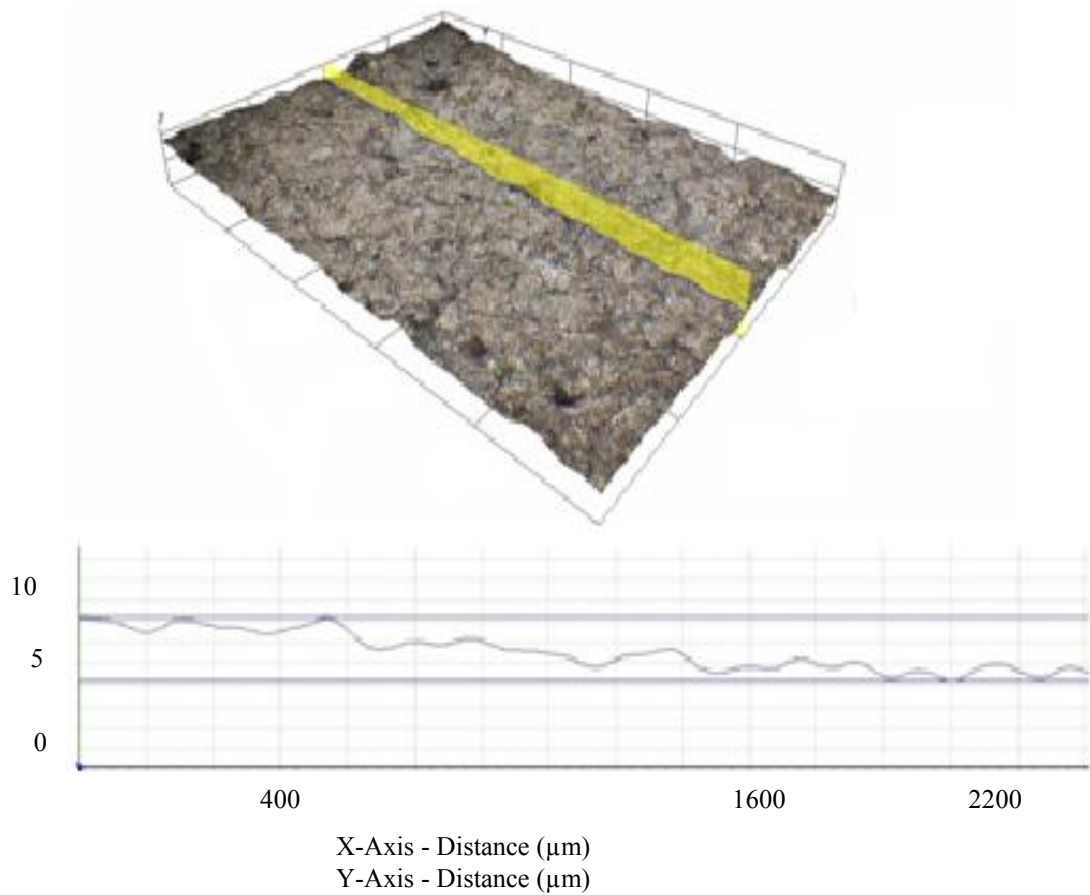


Figure 4.19 3-D Surface plot of Pt electrode showing 5.8 μm variation.

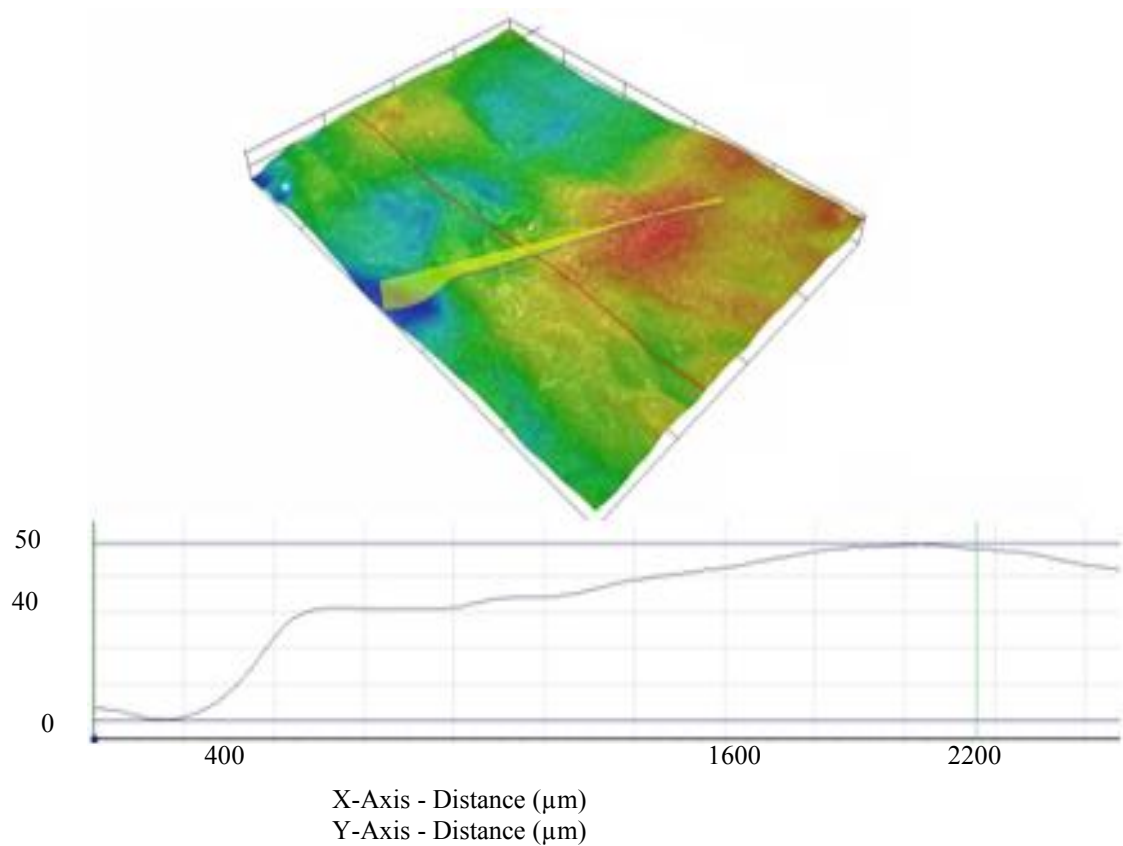


Figure 4.20 Pseudo color image of BP electrode showing 40 – 50 μm variation.

The electroless plating being a chemical process works on molecular levels to reduce the metal on to the surface of the polymer membrane. It is a surface phenomenon and hence shows very uniform plating and has very strong bonding. But the Bucky paper electrode assembled using the direct assembly process is a soft bonding. There is no very strong adhesion or cohesive force between the polymer matrix and the carbon nanotubes.

This uniformity also determines electric field on the IPMC actuator and hence directly influences the charge transfer. This allows for the accumulation of charges on various locations on the surface of the Bucky paper electrode.

The uniformity of the plating thickness was also studied. It is seen from Figure 4.20 that platinum electrodes plated using electroless plating technique are plated more uniform in thickness when compared to BP electrode formation using direct assembly. The variation in the thickness of the Pt electrode on a comparative basis from both the sides was 0.3 μm while the difference in the BP electrode thickness from one side to another was more than 40 μm .

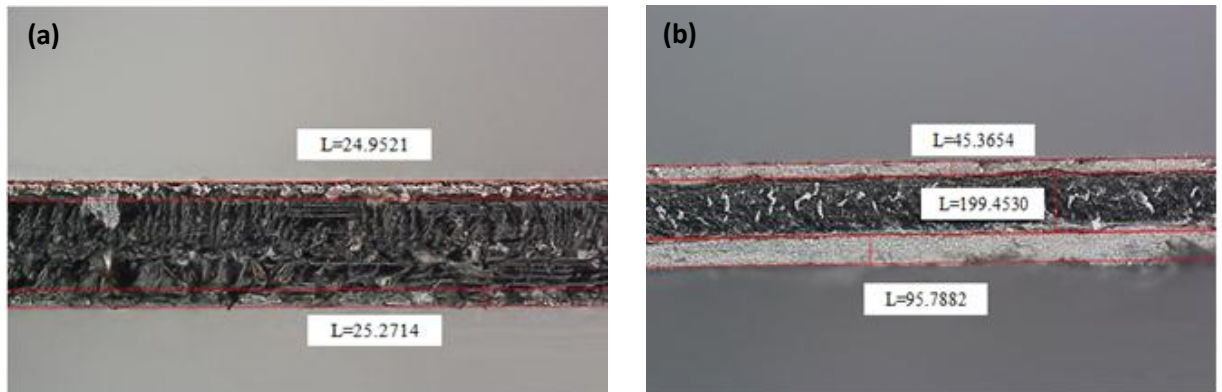


Figure 4.20 Cross sectional area of (a) Pt IPMC and (b) BP IPMC (L=Length in μm).

CHAPTER 5 Conclusion and Future work

The dissertation thesis presents novel methods for a manufacturing (i.e. development, analysis and comparison of electro mechanical properties) various IPMC samples with different electrodes and Ion content. Gold sputter coated electrodes, Bucky paper Direct Assembly Process electrodes and chemically plated platinum electrodes were compared and the failure of gold and Bucky paper IPMC electrodes were studied.

It was shown that the Gold sputter coated IPMC samples were not very efficient and failed after very few cycles and hence Bucky paper IPMC and platinum coated IPMCs were compared more in detail. The Bucky paper IPMC with Imidazolium ions were efficient when it came to current consumption and tip deflection whereas showed adverse results during the blocking force measurement. Since the smaller blocking force values might have been due to the constraints of the Imidazolium ion clusters passing through the sulfonate clusters within an actuating IPMC (i.e. the generally expanded cluster after swelling becoming deformed and causing constriction in the mobility of the cation within the polymer network) might have resulted in obtaining such values, it can be further enhanced by using smaller ionic fluids within the polymer structure to enhance the charge transport.

The tip displacements have shown satisfactory results when taken into consideration with the current consumption as a proof of the electromechanical efficiency of the BP (IM) IPMC sample.

The surface morphology studies were also performed in this paper that gives us a deeper insight into the polymer-electrode effective bonding. This work leads us further into changing the polymer matrix at material scale to further enhance the actuation properties of the IPMCs.

As future work, better manufacturing process of the IPMC electrodes have to be brought in place since the more efficient plating techniques are complicated and the easier plating techniques are not very efficient. By optimizing the product and process design we can further enhance the manufacturing of these IPMCs which would lead to shorter time in manufacturing and more efficient IPMC actuators. Other studies regarding reducing the evaporation of the water molecules within the IPMC when electric potential is applied and a more detailed FEM study of the electrode tip displacement have to be conducted. An efficient model to completely display the physics of the IPMC actuation has to yet be obtained on the finite element sector. This would be possible through obtaining better values for the composite polymer properties to be used on finite element.

REFERENCES

- [1] Smart Materials, A1 - Schwartz, M. SN - 9781420043730 UR (2014).
- [2] Relva C. Buchanan., "Heckman Diagram," *Ceramic Materials for Electronics*, Third Edition (2004).
- [3] Balaji Sivasubramanian., Daewon Kim., "Effects of Rapid Change in Temperature on Ultrasonic Guided Lamb Wave Propagation," *SMASIS2013-3173 pp. V002T05A011(2013)*.
- [4] American Piezo website, link: <https://www.americanpiezo.com/common-shapes-sizes/piezo-electrode-patterns.html> (2012).
- [5] Toshihiko Shiraishi, "Development of the control device using the intelligent material," *Journal of Intelligent Material Systems and Structures* (2005).
- [6] Popular mechanics, link : <http://www.popularmechanics.com/cm/popularmechanics/images/1Q/Detroit-TopTech-02-0113-1gn.jpg> (2013).
- [7] Bahramzadeh, Y. and Shahinpoor, M., "A Review of Ionic Polymeric Soft Actuators and Sensors," *Soft Robotics*, 1(1), 38-52 (2014).
- [8] Bar-Cohen, Y., Lei, H. and Tan, X. , "Fabrication and characterization of a two-dimensional IPMC sensor," *Electroactive Polymer Actuators and Devices (EAPAD)* (2013).
- [9] Bar-Cohen, Y., Ruiz, S. A., Mead, B., "Design optimization of rod shaped IPMC actuator," Proc. of SPIE Vol. 8687, 868722, *Electroactive Polymer Actuators and Devices (EAPAD)* (2013).
- [10] Chen, I. W. P., Cottinet, P.-J., Tsai, S.-Y., "Improved performance of carbon nanotube buckypaper and ionic-liquid-in-Nafion actuators for rapid response and high durability in the open air," *Sensors and Actuators B: Chemical*, (2012).
- [11] Mohsen Shahinpoor and Kwang J. Kim, "Ionic Polymermetal Composites: I. Fundamentals," *Smart Mater. Struct.*,10, 819-833 (2001).
- [12] Bhandari, B., Lee, G.-Y. and Ahn, S.-H., "A review on IPMC material as actuators and sensors: Fabrications, characteristics and applications," *International Journal of Precision Engineering and Manufacturing*, 13(1), 141-163 (2012).
- [13] Gierke, T. D.; Hsu, W. Y., "Perfluorinated Ionomer Membranes," *ACS Symposium Series*, Chapter 13, p 283 (1982).
- [14] Kazuo Onishi., Shingo Sewa., Kinji Asaka., Naoko Fujiwara., and Keisuke Oguro, "Morphology of Electrodes and BendingResponse of the Polymer Electrolyte Actuator," *Electrochimica Acta*, 46, 737-743 (2000).
- [15] Akle, B. J., Bennett, M. D., Leo, D. J. et al., "Direct assembly process: a novel fabrication technique for large strain ionic polymer transducers," *Journal of Materials Science*, 42(16), 7031-7041 (2007).

- [16] Chen, Z., Um, T. and Bart-Smith, H. "Ionic Polymer-Metal Composite Artificial Muscles in Bio-Inspired Engineering Research: Underwater Propulsion," *Smart Actuator systems*, (2012).
- [17] Cottinet, P. J., Souders, C., Labrador, D. et al., "Nonlinear strain–electric field relationship of carbon nanotube buckypaper/Nafion actuators," *Sensors and Actuators A: Physical*, 170(1-2), 164-171 (2011).
- [18] Cottinet, P. J., Le, M. Q., Degraff, J. et al., "Strain phenomenon in carbon nanotube buckypaper actuator: Experiments and modeling," *Sensors and Actuators A: Physical*, 194, 252-258 (2013).
- [19] B. Mead; S. Ruiz; W. Yim., "Closed-loop control of a tube-type cylindrical IPMC" Proc. SPIE 8687, *Electroactive Polymer Actuators and Devices (EAPAD)* (2013).
- [20] D. Pugal, K. J. Kim and a. A. Aabloo, "An explicit physics-based model of ionic polymer-metal composite actuators," *Journal of Applied Physics*, (2011).
- [21] E. Shoji and D. Hirayama, "Effects of Humidity on the Performance of Ionic Polymer–Metal Composite Actuators: Experimental Study of the Back-Relaxation of Actuators," *Journal Oh Physical Chemistry*,(2007).
- [22] M. Otis, R. Bemierl, Y. Pasco, H. MCnard, H. Semmaoui, M. Jany and R. Fontaine, "Development of an Hexapod BioMicroRobot with Nafion-Pt IPMC Microlegs," in *International conference of the IEEE EMBS*, Cancun, (2003).
- [23] L. Fortuna, P. Brunetto, S. Graziani, G. Dongola, R. Caponetto, "A Scalable Fractional Model for IPMC actuator", *PHYSCON*, Italy (2009).
- [24] T. Mirfakhrai., J.D.W. Madden, R.H. Baughman., "Polymer artificial muscles," *Materials Today*, April (2007).
- [25] J. D. W. Madden, N. A. Vandesteeg, P. A. Anquetil, P. G. A. Madden, A. Takshi, R. Z. Pytel, S. R. Lafontaine, P. A. Wieringa and I. W. Hunter, "Artificial muscle technology: physical principles and naval prospects," *IEEE Journal of Oceanic Engineering*, vol. 29, no. 3, pp. 706-728, (2004).